

Infield Response of $(Ag)_x/CuTl-1223$ Nanoparticles- Superconductor Composites



By

Muhammad Waqas Rabbani
(268-FBAS/MSPHY/S14)

Supervisor:

Dr. Muhammad Mumtaz

Assistant Professor
Department of Physics, FBAS,
IIU, Islamabad

Department of Physics
Faculty of Basic and Applied Sciences
International Islamic University, Islamabad
(2016)



Accession No TH-16335

K
M-*[Signature]*

MS
527.623
RAI



Infield Response of (Ag)_x/CuTl-1223 Nanoparticles-Superconductor Composites

by:

Muhammad Waqas Rabbani
(268-FBAS/MSPHY/S14)

This Thesis submitted to Department of Physics International Islamic University,
Islamabad, for the award of degree of MS Physics.



Chairman Department of Physics

International Islamic University, Islamabad

CHAIRMAN
DEPT. OF PHYSICS
International Islamic University
Islamabad




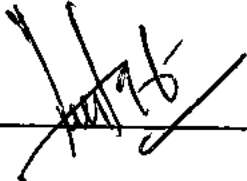
Dean Faculty of Basic and Applied Sciences
International Islamic University, Islamabad.

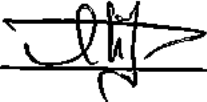
Final Approval

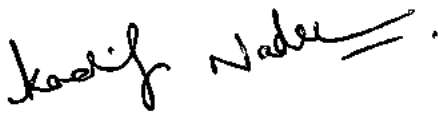
It is certified that the work presented in this thesis entitled “Infield response of (Ag)_x/CuTl-1223 nanoparticles-superconductor composites” Muhammad Waqas Rabbani Registration No. 268-FBAS/MSPHY/S14 fulfills the requirement for the award of degree of MS Physics from Department of Physics, International Islamic University, Islamabad, Pakistan.

Viva Voce Committee

Chairman 
(Department of Physics) 2.3.16

Supervisor 

External Examiner 

Internal Examiner 



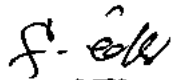
DEDICATED

To

*The person who is eradicating Cancer from the
country*

Declaration of Originality

I, **Muhammad Waqas Rabbani** Registration No. 268-FBAS/MSPHY/S14 student of MS Physics (Session 2014-2016), hereby declare that the work presented in the thesis entitled “**Infield response of $(Ag)_x/CuTi-1223$ nanoparticles-superconductor composites**” in partial fulfillment of MS degree in Physics from International Islamic University, Islamabad, is my own work and has not been published or submitted as research work or thesis in any form in any other university or institute in Pakistan or abroad.


Muhammad Waqas Rabbani
(268-FBAS/MSPHY/S14)

Dated: 21-03-18

Forwarding Sheet by Research Supervisor

The thesis entitled “Infield response of $(Ag)_x/CuTl-1223$ nanoparticles-superconductor composites” submitted by Muhammad Waqas Rabbani (Registration No. 268-FBAS/MSPHY/S14) in partial fulfillment of MS degree in Physics has been completed under my guidance and supervision. I am satisfied with the quality of his research work and allow him to submit this thesis for further process to graduate with Master of Science degree from Department of Physics, as per International Islamic University, Islamabad rules and regulations.


Dr. Muhammad Mumtaz

Assistant Professor
Department of Physics,
International Islamic University,
Islamabad

Dated: 02/03/2016

Acknowledgement

I have no words to express my deepest sense of gratitude and numerous thanks to Almighty Allah, who enabled me to complete this study and with innumerable blessings for the Holy Prophet Peace Be Upon Him who is forever a torch of guidance and knowledge for the whole humanity.

I would like to thank my supervisors Dr. Muhammad Mumtaz, whose personal interest, thought provoking guidance, valuable suggestions and discussions enabled me to complete this work. I am certain that the guidance and training provided by her to me has laid a foundation for my future success. I would like to pay lots of appreciation to all my teachers, especially Dr. Kashif Nadeem who blessed me with knowledge and guidance.

I deem it utmost pleasure to express my heartiest gratitude to my amiable senior lab fellows for their kind support, guidance and care which help me put-up with all the frustration encountered during my research work and also for their pleasant companionship. Especially I will not forget the great role of Ghulam Hussain, Abdul Jabar Bhutta, Irfan Qasim, Liaqat Ali, Waqee-ur-Rehman, Faisal Zeb, Syed Qamar Abbas and Ghulam Abbas who facilitated me by their humble guidance whenever I require during the period. I am indeed humbly grateful to them for their kind attitude, valuable suggestions, most cooperative affectionate behavior, guidance and moral help. I feel great pleasure in expressing my heartiest thanks to my dearest friend Abdul Wahab and Awwais Bhatti, who shared all my sorrows and happiness and for being there whenever I needed any help.

Last but not the least I am highly indebted to my Parents, their continuous support, positive attitude and encouragement greatly motivated me throughout my educational career. They prayed for me, shared the burdens and made sure that I sailed through smoothly.

I thank again ALMIGHTY ALLAH, who listens and responds to my every prayer.

Muhammad Waqas Rabbani

Table of Contents

| | |
|---|----|
| Chapter 1 : Introduction..... | 1 |
| 1.1 Historical review of superconductivity..... | 1 |
| 1.2 Basic Properties of Superconductivity..... | 2 |
| 1.2.1 Zero Electrical Resistance..... | 2 |
| 1.2.2 Missner Effect..... | 3 |
| 1.2.3 Critical parameters in superconductors..... | 5 |
| 1.3 The development of superconducting materials..... | 5 |
| 1.3.1 Copper thallium based superconductor..... | 7 |
| 1.4 Vortex matter in high T_c superconductors..... | 8 |
| 1.4.1 Vortex Motion..... | 9 |
| 1.4.2 Flux Creep..... | 10 |
| 1.4.3 Phase Diagram..... | 10 |
| 1.4.4 Vortex liquid..... | 12 |
| 1.4.5 Vortex solid..... | 13 |
| 1.5 Aims and objectives of research..... | 14 |
| References..... | 15 |
| Chapter 2: Thermally Assisted Flux Flow and Literature Review..... | 20 |
| 2.1 Thermally assisted flux flow (TAFF)..... | 20 |
| 2.2 Effect of nanostructures inclusion in HTSCs..... | 21 |
| References..... | 26 |
| Chapter 3: Synthesis and Characterization Techniques..... | 28 |
| 3.1 Nanoparticles synthesis..... | 28 |
| 3.1.1 Ag nanoparticles synthesis..... | 28 |
| 3.1.2 Synthesis of $Cu_{0.5}Ba_2Ca_2Cu_3O_{10-\delta}$ precursor..... | 30 |
| 3.1.3 Synthesis of $(Ag)_x/CuTl-1223$ nanoparticles superconductor composite..... | 31 |
| 3.2 Characterization Techniques..... | 32 |
| 3.2.1 X-rays diffraction (XRD)..... | 32 |
| 3.2.1.1 Basic principle..... | 32 |
| 3.2.1.2 Bragg's law..... | 33 |
| 3.2.1.3 Powdered diffraction method..... | 34 |
| 3.2.1.4 X-rays diffractometer instrument..... | 34 |
| 3.2.1.5 XRD Applications..... | 34 |

| | |
|---|-----------|
| 3.2.2 Scanning electron microscope (SEM)..... | 35 |
| 3.2.2.1 Components of SEM | 35 |
| 3.2.3 Resistivity measurements by Four-probe method..... | 37 |
| References | 39 |
| Chapter 4: Results and Discussion..... | 41 |
| 4.1 X-Ray diffraction analysis | 41 |
| 4.2 Scanning electron microscopy (SEM) | 42 |
| 4.3 Resistive transition..... | 43 |
| 4.4 Activation energy..... | 45 |
| 4.5 Upper critical field H_{c2} and irreversibility field H_{irr} | 46 |
| Conclusions..... | 50 |
| References | 51 |

List of Figures

| | |
|--|---|
| <p>Fig. 1.1: Meissner affect for Type I superconductor in magnetic field with one critical transition field H_c (a) and (b) for Type II superconductor in magnetic field with two critical transition fields lower critical field H_{c1} and upper critical field H_{c2}. ..4</p> <p>Fig. 1.2: Critical surface phase diagram of superconductor composed by critical transition temperature T_c, critical transition field H_c, and critical current density J_c..... 5</p> <p>Fig. 1.3: History of superconductor's development with year.....7</p> <p>Fig. 1.4: Crystal structure of CuTl-1223.....7</p> <p>Fig. 1.5: Flux bundles jump between adjacent pinning centers. When no current is applied, the probability of jumping is the same in all directions. An electrical current induces a flux density gradient that favors the jumps in one direction. In this schematic view, the free energy is shown as a function of the position of the bundle.10</p> <p>Fig. 1.6: The phase diagram show: (a) the type II superconductor under influence of external magnetic field and three phases present in a conventional superconductor. (b) Shows the HTSc with vortex liquid and vortex solid regime.11</p> <p>Fig.1.7: Schematic plot of resistivity ρ versus current density j for a superconductor. At high temperatures the pinning barriers are much smaller than thermal energy and the system is in the flux flow regime (FF). As T decreases and the system gets closer to the solid phase, the pinning barriers become large compared to the thermal energy (TAFF regime). In the solid the resistivity comes from creep motion of the vortices.....12</p> <p>Fig. 2.1: Arrhenius plot of normalized resistance for the YBCO single crystal, in magnetic fields $B \parallel c$ at 0, 0.5, 1, 2, 4, 6, 9 and 12 T (left to right). The dashed line marks the crossover from flux flow at high temperatures to TAFF at low resistivity21</p> <p>Fig. 3.1: Systematic diagram of physical and chemical methods for nanoparticles synthesis.....28</p> <p>Fig. 3.2: Flow chart of Ag nanoparticle synthesis.29</p> <p>Fig. 3.3: Schematic flow chart of synthesis of $Cu_{0.5}Ba_2Ca_2Cu_3O_{10-\delta}$ precursor.30</p> | <p>4</p> <p>5</p> <p>7</p> <p>7</p> <p>10</p> <p>11</p> <p>12</p> <p>21</p> <p>28</p> <p>29</p> <p>30</p> |
|--|---|

| | |
|---|----|
| Fig. 3.4: Schematic diagram of $(Ag)_x/CuTl-1223$ nanoparticle superconductor composite..... | 31 |
| Fig. 3.5: Working mechanism of XRD..... | 33 |
| Fig. 3.6: Diffraction of X-rays from crystal planes and illustration of Bragg's Law. . | 33 |
| Fig. 3.7: Labeled diagram of X-ray diffractometer..... | 34 |
| Fig. 3.8: Labeled diagram of scanning electron microscope (SEM). | 35 |
| Fig. 3.9: Schematic diagram of scanning electron microscope. | 37 |
| Fig. 3.10: Labeled diagram of four point probe apparatus (R-T measurements)..... | 38 |
| Fig. 4.1: XRD spectra of $(Ag)_x/(CuTl-1223)$ nanoparticles-superconductor composites with $x = 0, 2$ and 4 wt. % | 41 |
| Fig. 4.2: Scanning electron microscopy (SEM) of $(Ag)_x/CuTl-1223$ composites with (a) $x = 0$, (b) $x = 0.5$ wt. %, (c) $x = 1$ wt. %, (d) $x = 2$ wt. % and (e) $x = 4$ wt. % .. | 42 |
| Fig. 4.3: The magnetic field dependence of resistivity as the function of temperature for $(Ag)_x/CuTl-1223$ nanoparticles-superconductor composites ($x = 0, 0.5, 1.0, 2.0$ and $x = 4.0$ wt. %) at $H = 0, 2, 4, 6$ and 8 T. The inset shows the Arrhenius plots of resistive transition and linear part of low resistivity region is fitted to obtain the activation energy..... | 44 |
| Fig. 4.4: Activation energy versus applied magnetic field plot of $(Ag)_x/CuTl-1223$ nanoparticles-superconductor composites ($x = 0, 0.5, 1.0, 2.0$ and $x = 4.0$ wt. %) | 45 |
| Fig. 4.5: The plot applied field H (T) versus Temperature T (K) for the point where resistivity drop to 90%, 50% and 10% of normal state resistivity ρ_n for $(Ag)_x/CuTl-1223$ nanoparticles-superconductor composites ($x = 0, 0.5, 1.0, 2.0$ and $x = 4.0$ wt. %)..... | 47 |
| Fig. 4.6: The value of $H_{c2}(0)$ and $\xi(0)$ for $(Ag)_x/CuTl-1223$ nanoparticles-superconductor composites..... | 48 |

List of Tables

| | |
|---|----|
| Table 4.1: The magnetic field dependent activation energy $U_0(H)$ is calculated from Arrhenius plots | 46 |
| Table 4.2: Measured superconducting parameters for $(Ag)_x/CuTl-1223$ nanoparticles-superconductor composites..... | 49 |

Abstract

Superconducting transition and pinning properties of $(Ag_x)/CuTi-1223$ nanoparticles-superconductor composites ($x = 0, 0.5, 1.0, 2,$ and 4.0 wt.%) was investigated at different magnetic field up to $H = 8$ T. The overall increase in critical temperature (T_c) was observed and found maximum for $x = 2.0$ wt.%. The values of T_c^{onset} remained unaffected by applying the magnetic field, but at low temperature critical temperature T_c decreased by increasing the magnetic field. The normal state resistivity ρ_n decreased, which is the confirmation of improvement in inter-grain connectivity after the addition of Ag nanoparticles. The transition region at low temperature shows the Arrhenius behavior due to thermally activated flow of vortices. Modified form of Arrhenius law was used to analyze thermally activated activation energy (U_0). The critical temperature T_c , activation energy U_0 , and upper critical field H_{c2} were found to be optimized for $x=2.0$ wt.%.

Chapter 1 : Introduction

1.1 Historical review of superconductivity

Superconductivity is one of the most attractive topic in natural science/ Since 1913, the Royal Swedish Academy of Science has award the Noble Prize of Physics for five times to the achievements on superconductivity.

First one was won in 1913 by H. K. Onnes [1]. Although the official announced prize winning reason is for the investigations of electrical properties of matter at low temperatures that were produced by liquid helium, everyone knows the work marked the discovery of superconductivity by observing the zero dc electric resistivity in pure mercury below 4.2K. In 1972, the prize was awarded to J. Bardeen, L. N. Cooper and J. R. Schrieffer for developing the theory of superconductivity that is known as BCS theory [2, 3]. The theory described superconductivity as a microscopic effect caused by a Bose-Einstein condensation of special electron pairs, namely Cooper pairs. The formation mechanism of Cooper pair is based on the interaction between electrons and crystal lattice.

Continuously, I. Giaever and B. D. Josephson were won the shared Nobel Prize in 1973. Giaever was awarded for his experimental discoveries concerning tunneling phenomena in superconductors [4] and Josephson was selected due to his theoretical predictions on a microscopic quantum phenomenon of a supercurrent through a tunnel barrier [5]. These works opened a wide field to applications of superconductors. The discovery of superconductivity in ceramic materials hit the Noble Prize of Physics in 1987. J. G. Bednorz and K. A. Muller detected the metal-superconductor transition on a lanthanum barium copper oxide (LaBaCuO) at 35 K that was a breakthrough in critical transition temperature of superconductors [6]. This work marked the beginning of the era of high temperature superconductivity.

The most recent success was achieved by V. L. Ginzburg and A. A. Abrikosov, who were two out of three winners of Noble Prize of Physics in 2003. Ginzburg was awarded for his contribution in establishing Ginzburg- Landau Theory that is a phenomenological model to describe phase transition of superconductors based on thermodynamic interpretation. Abrikosov was awarded due to describe the vortex lattice in type-II superconductors [7, 8].

The development in the field of superconductivity, including the great achievements above mentioned, not only promoted the progress in related disciplines, such as condensed matter physics, quantum physics, material science and so on: but also created a series of applications based on superconductors special properties of electricity and magnetism, such as power transport, magnetic resonance imaging and so on. In future, it is foreseeable that if the new break through are obtained in mechanism of high temperature superconductivity or of superconductors working at room temperature and atmospheric pressure, the Noble Prize of Physics will probably be granted to these works in the field of superconductivity again.

1.2 Basic Properties of Superconductivity

Besides the sudden disappearance of electrical DC resistance, superconductors have some universal properties that are independent of the materials themselves. The existence of these universal properties indicates that superconductivity is a thermodynamics phase.

1.2.1 Zero Electrical Resistance

An electrical current in conductor may be described as a cloud of electrons flowing across a heavy ionic lattice. During current transporting, the electrons constantly collide with the nodes (ions) of the lattice, and in each collision consumes some of the energy carried by the current and converted it into heat. As a result, the energy carried by the current is constantly being dissipated. This is the phenomenon of electrical resistance, which is given by Ohm's law.

However, the situation is totally different in a superconductor since no voltage is required to maintain the transport current. According to BCS theory, the electronic fluid cannot be resolved into individual electrons in a superconductor. Instead, current carriers are formed by the bound pairs of electrons is produced by the energy exchange from phonons. Due to quantum mechanics, the Cooper pair fluid possesses a special energy gap that is larger than the thermal energy of the lattice. Thus, the fluid will not be scattered by the lattice and performance as a superfluid, meaning it can move without energy dissipation. Although BCS theory gives microscopic description of zero resistance in conventional superconductors, it cannot explain the phenomenon in high temperature superconductors (HTSCs). In these cases, the energy gap belonging to Cooper pairs have been less than the thermal energy of the lattice at

temperatures not too far below the nominal superconducting transition: whereas experiments have demonstrated that currents in HTSCs coils also can persist for long time without any measurable degradation.

1.2.2 Meissner Effect

In 1933 Walther Meissner and Robert Ochsenfeld observed that the field strength outside a sample increased as it became superconducting. It was soon realized that what they were indirectly observing was the sample becoming a perfect diamagnetic and expelling the penetrating field. The Meissner effect is simple to illustrate: above T_c , magnetic flux flows through a bulk sample in its normal state, as shown in Fig 1.1 and as the temperature is lowered past T_c the flux is expelled and forced around the superconducting sample, as shown in Fig. 1.1(b).

The Meissner effect was given a phenomenological explanation by the brother Fritz and Heinz London, who showed that the electromagnetic energy in a superconductor is minimized provided

$$\Delta^2 H = \lambda^{-2} H \dots\dots\dots 1.1$$

where H is the magnetic field and λ is the London penetration depth [9]. This equation, which is known as the London equation, predicts that the Meissner effect does not cause the field to be completely ejected but instead the field penetrates the superconductor only a very small distance λ , decaying exponentially to zero within the bulk of the material. The Meissner effect is a defining characteristic of superconductivity. For most superconductors the London penetration depth is on the order of 100 nm.

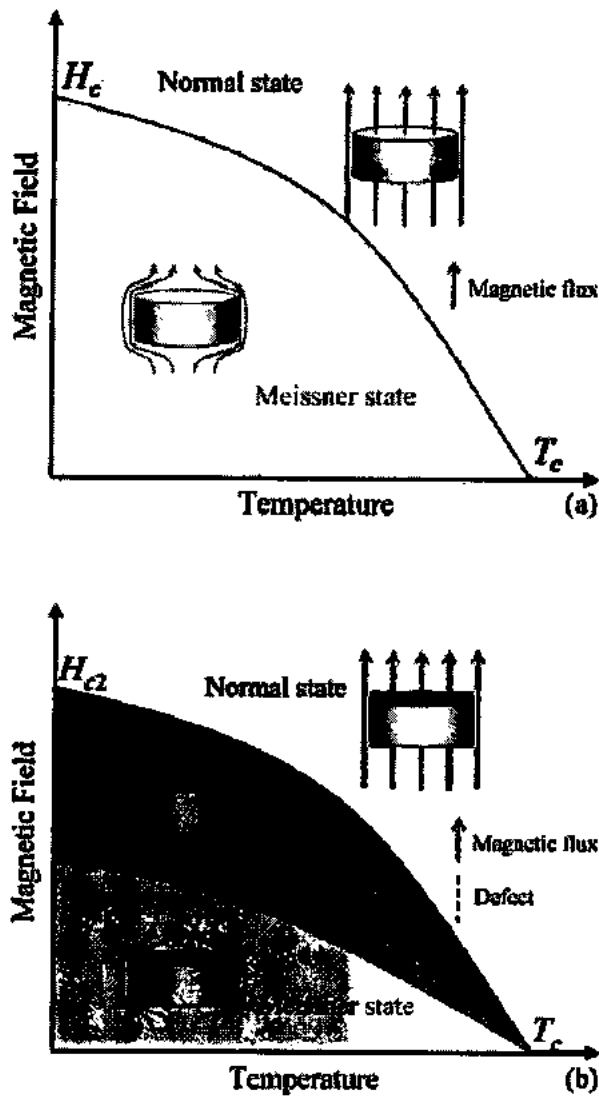


Fig. 1.1: Meissner affect for Type I superconductor in magnetic field with one critical transition field H_c (a) and (b) for Type II superconductor in magnetic field with two critical transition fields lower critical field H_{c1} and upper critical field H_{c2} [10].

The Meissner effect breaks down when the applied magnetic field is larger than the critical magnetic field. Superconductors can be divided into two classes according to how this breakdown occurs as shown in Fig. 1.1. In Type I superconductors, superconductivity is abruptly destroyed when the strength of the applied field rises above a critical value H_c . In Type II superconductors, raising the applied field past a lower critical value H_{c1} leads to a mixed state in which an increasing amount of magnetic flux penetrates the materials, but there remains no resistance to the flow of electrical current, as long as the current is not too large. At upper critical field strength H_{c2} , superconductivity is destroyed. Most pure elemental superconductors, except niobium, technetium and vanadium etc., are Type I, while all impure and compound superconductors are Type II.

1.2.3 Critical parameters in superconductors

Based on the elementary properties of superconductors, the superconducting state depends on three parameters: temperature, magnetic field and current density. Every parameter has a critical value to divide the normal state and superconducting state in a particular superconductor. It is necessary for the superconducting state that the temperature is lower than the critical temperature T_c . Any current and external magnetic field which exceed the critical current density J_c and critical magnetic field H_c will also destroy superconducting state. The relationship of three parameters is shown in Fig 1.2 the superconducting state is under the surface formed by the T_c , J_c and H_c .

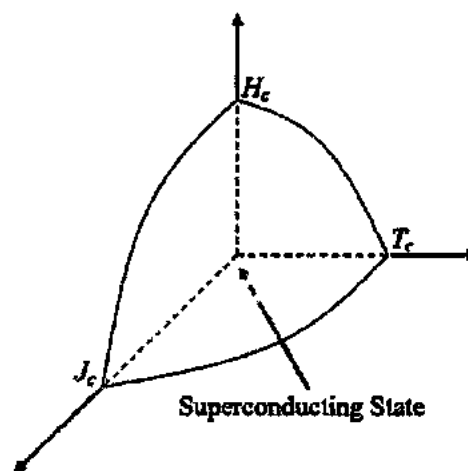


Fig. 1.2: Critical surface phase diagram of superconductor composed by critical transition temperature T_c , critical transition field H_c , and critical current density J_c [11].

1.3 The development of superconducting materials

Since the discovery of superconductivity by H. K. Onnes in 1911[1], the development of superconducting materials is a long and ruded road to pursue high T_c approaching room temperature. It is well known, superconductivity was first discovered in Hg at 4.2K. in 1911, lead was found to be superconductor at 7K. In subsequent decades, superconductivity was found in several types of materials, such as pure elements, alloys, intermetallic compounds, ceramics etc. They are classified into three categories as shown in Fig 1.3.

Until 1973, the highest T_c of 23.2 K was found in Nb_3Ge [12, 13]. This record held until 1986, when $La_{1-x}BaCu_2O_4$ was found to be superconductive with T_c up to 35K [14]. Later in early 1987, $Yba_2Cu_3O_7$ (YBCO) was found to have T_c up to 93K [15, 16] making it possible to utilize low cost liquid nitrogen (boiling point at 77K)

as the refrigerant. Now, superconductors with T_c below 23K are collectively called low temperature superconductors (LTSCs) while with the T_c above 23K are called high temperature superconductors (HTSCs) [17].

The discovery of high temperature superconductivity in cuprates attracted numerous attentions, several typical copper based HTSCs were found in the following decade. In 1988, a high T_c of about 105K was obtained in a Bi-Sr-Ca-Cu-O (BSCCO) combination [18, 19]. In early 1988 the Tl-Ca/Ba-Cu-O system with T_c up to 120K was found [20]. In 1993, $\text{HgBa}_2\text{CuO}_{4-x}$ with T_c of 94K was discovered as the first Hg-based cuprate superconductor [21] and then a higher T_c up to 134K was found in $\text{HgBa}_2\text{Ca}_2\text{Cu}_3\text{O}_{8-x}$ (Hg-1223) at ambient pressure [22]. In 1994, the highest T_c of 164K, which remains the world record now, was achieved in Hg-1223 under 31GPa quasi hydrostatic pressure [23]. A new HTSc with critical temperature T_c up to 132K was developed in 2001 with combination of Cu and Tl systems by H. Ihara and fellows [24]. They developed the selective reduction for hole-doping for $\text{Cu}_{1-x}\text{Tl}_x\text{Ba}_2\text{Ca}_3\text{Cu}_4\text{O}_{12-y}$ (CU_{1-x}Tl_x-1234) and $\text{Cu}_{1-x}\text{Tl}_x\text{Ba}_2\text{Ca}_2\text{Cu}_3\text{O}_{10-y}$ (CU_{1-x}Tl_x-1223) system.

In 2001, a binary inter metallic compound MgB_2 was found with the T_c 39K [25]. This discovery created great interest in both research and industrial applications due to the simple structure of MgB_2 and low cost of raw sources. After several year developments, MgB_2 wires produced by the power-in-tube method have become a very possible alternative for the commercially used LTSCs Nb_3Sn and NbTi [26].

In February 2008 fluorine doped $\text{LaFeAsO}_{1-x}\text{F}_x$ was found to be superconducting with T_c of 26K [27]. One month later, a higher T_c of up 55K was obtained in $\text{SmFeAsO}_{1-x}\text{F}_x$ compound [28]. The Fe-layer based noncuprate HTSCs has become a hot research point in the field of superconductivity, which is still going in today [29]. Experts hope that having another family to study will also help to develop a theory of the cuprate superconductors.

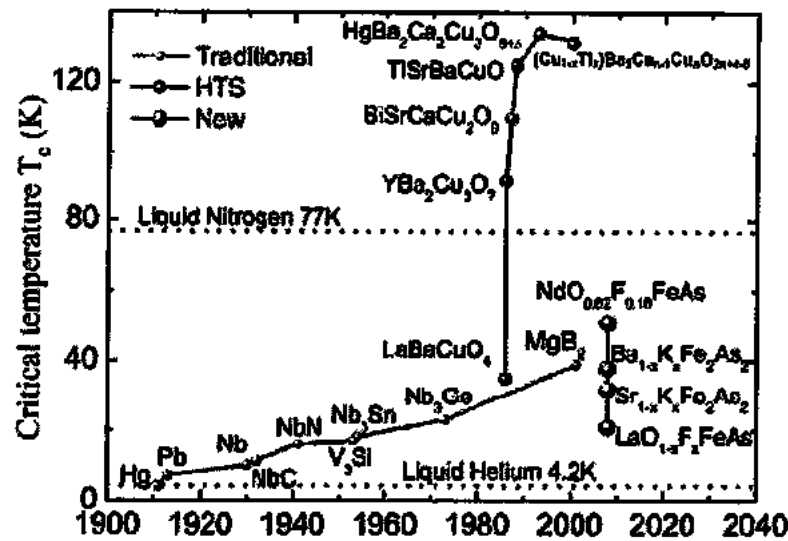


Fig. 1.3: History of superconductor's development with year.

1.3.1 Copper thallium based superconductor

$\text{CuBa}_2\text{Ca}_{n-1}\text{O}_{2n-1}\{\text{Cu}-12(n-1) \text{ n, n} = 1, 2, 3, 4, \dots\}$ exhibits the tetragonal structure and high pressure is needed for its synthesis. It has high critical current density and high critical temperature is about 120 K. In these superconductors, if it is added thallium with it then a new family of superconductor comes into being which is known as CuTl-1223 superconductor having critical temperature is about 132K and crystal structure is shown in Fig. 1.4. The structure of these superconductors has two divisions, a charging reservoir and a superconducting block which provides charge carriers to planes. [24, 30-32].

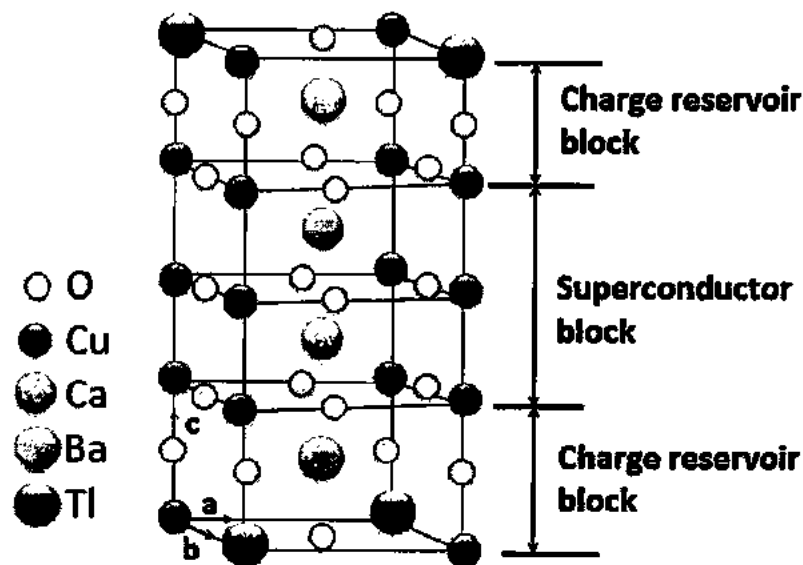


Fig. 1.4: Crystal structure of CuTl-1223.

1.4 Vortex matter in high T_c superconductors

High conductor superconductors are type II materials: they have long penetration length λ and short coherence lengths ξ , as a result in large value of the Ginzburg Landau parameter κ . A direct effect of larger value of κ is that the mixed state extended over a large region of H-T phase diagram. This is also clear when we observe the expressions for the lower and upper critical field. The magnetic flux will start to penetrate in the superconductor when the Gibbs free energy of one vortex becomes larger than the Gibbs energy present in Meissner pure state. The vortex starts penetrating just above the lower critical field H_{c1} .

$$H_{c1} = \frac{\phi_0}{4\pi\mu_0\lambda^2} \ln \frac{\lambda}{\xi} \dots\dots\dots 1.2$$

A long coherence depth λ leads to low value of H_{c1} and therefore the Meissner state in HTS remains in a small region. While in upper critical field region H_{c2} the numbers of vortices are high and their cores start to overlap. The H_{c2} is found by using the Ginzburg-Landau theory.

$$H_{c2} = \frac{\phi_0}{2\pi\mu_0\xi^2} \dots\dots\dots 1.3$$

So the H_{c2} value is larger for a short coherence length ξ in superconductors. In phase diagram for HTS, the vortex state occupies a large region.

In a pure sample the vortices are in an arranged manner and super-current create the repulsive forces which keep the vortices apart from each other and help to push out from the materials. However, at fields above H_{c1} the energy is lowest in the presence of vortices, so a force will appear to keep the flux density constant by preventing the vortices from leaving the sample. The equilibrium between these forces is established and vortices are remaining in an arranged form.

The vortex lattice is also known as Abrikosov lattice, due to the discovery by Alexei Abrikosov in 1957 of a solution to the linearized Ginzburg-Landau equation that predicted a lattice of parallel flux lines [33]. The first image of Abrikosov lattice was taken by Essmann and Trauble in 1967 using Bitter decoration on Pb-4 [34]. After the discovery YBCO superconductor Gammel used the same technique to observe the lattice [35]. Many other techniques have been used successfully to image the vortices, such as tunneling microscopy or magnetic force microscopy [36]. Vortex

dynamics haven been also directly studied by using Lorentz microscopy and magneto-optical techniques [37].

1.4.1 Vortex Motion

Vortices are in motion, when a current density j is applied to a superconductor in mixed state then the Lorentz force will appear. The force exerted on per unit length of vortex is

$$f_L = j \times \phi_0 \dots\dots\dots 1.4$$

Where $\phi_0 = \phi_0 \hat{z}$, assuming that vortices are parallel to the z axis. . The Lorentz force per unit volume over the entire sample is $F_L = j \times B$, where B is the mean flux density. A viscous drag force opposes the vortex flow and gives a constant velocity v of the vortices. The viscous drag force per unit length on a vortex is

$$f_\eta = \eta v \dots\dots\dots 1.5$$

where η is viscous drag coefficient. The perfect conductivity is lost due to power dissipation in the vortex system which is generated from the motion of vortices by an electric field $E = B \times v$ which is parallel to j .

Another force is necessary in order to keep the vortices from moving even when $F_L \neq 0$ and in that way to recover perfect conductivity. In real materials, this extra force comes from the static disorder present in the system. For a vortex it is convenient to be located in a defect, as the order parameter is already depressed there and it is not necessary to create a whole normal core. However, a random distribution of point pinning centers will not be effective to pin a rigid vortex lattice, since the sum of the individual pinning forces from each pinning site would add up to zero. In 1979, Larkin and Ovchinnikov studied this problem in their theory of collective pinning [38].

The property of dissipation free current flow is recovered when vortices are pinned by disorder. However, if current density is increased above the critical current density value j_c , the Lorentz force will overcome the pinning force and the vortices will start moving again. This depinning critical current density j_c is bounded by the current at which the Cooper pairs are destroyed, known as the depairing current density j_0 , so $j_c < j_0$. Pinning is most effective at low temperatures, where thermal fluctuations are not as important, so at higher temperatures the flux lines can be depinned at current densities smaller than j_c .

1.4.2 Flux Creep

At high temperatures, the thermal energy may be sufficient to allow flux lines to jump from one pinning center to another; even the current density is not larger than j_c . Flux bundles jump between adjacent pinning points in a process known as flux creep, explained in the theory developed by P. W. Anderson and Y. B. Kim [39, 40]. The jump rate is given by

$$\mathfrak{R} \propto e^{-U_0/k_B T} \dots\dots\dots 1.6$$

where U_0 is the activation energy of the pinning barrier. If no current is applied, the probability of jumping is the same in all directions and no creep is observed. A current will induce a flux density gradient favoring the jumps in the direction in which the flux density decreases, as shown schematically in Fig. 1.5. The electric field caused by the flux creep is [41].

$$E(j) \propto e^{-U_0/k_B T} \sinh\left(\frac{jU_0}{j_c k_B T}\right) \dots\dots\dots 1.7$$

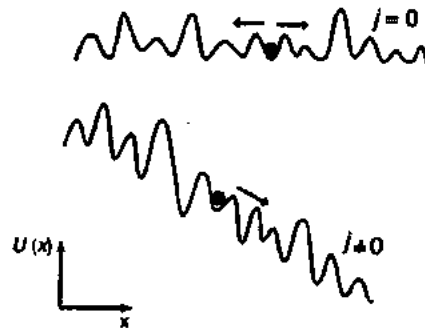


Fig. 1.5: Flux bundles jump between adjacent pinning centers. When no current is applied, the probability of jumping is the same in all directions. An electrical current induces a flux density gradient that favors the jumps in one direction. In this schematic view, the free energy is shown as a function of the position of the bundle [41].

1.4.3 Phase Diagram

The superconductor system gains energy due to motion of vortices under the influence of the Lorentz force. If this energy is smaller than the pinning energy, the vortices will be trapped by the defects present in the system. But for the pinning to be effective, the vortex lattice has to adapt to the pinning landscape at the cost of some elastic energy. Thermal energy also plays an important role: at high enough temperatures, the pinning barriers become irrelevant compared to the thermal energy (flux flow regime), and thermal activation is also responsible to makes the creep and

TAFF phenomena possible. The competition between elastic, pinning and thermal energies shapes the phase diagram of high-temperature superconductors.

The importance of thermal fluctuations is measured by the Ginzburg number G_i

$$G_i = \frac{1}{2} \left(\frac{\gamma k_B T}{4\pi\mu_0 H_c^2 \xi_{ab}^3(0)} \right)^2 \dots\dots\dots 1.8$$

where γ is the mass anisotropy parameter, $\xi_{ab}(0)$ is the coherence length along the ab plane and H_c is the thermo dynamical critical field, $H_c = \phi_0 / (2\sqrt{2} \pi\mu_0 \lambda \xi)$. The large anisotropy parameter γ , short ξ and high T_c characteristic of HTS a large G_i and very soft vortex matter, giving rise to a very rich phase diagram.

In these materials, thermal fluctuations are important enough to overcome the elastic energy of the vortex lattice in a large part of the phase diagram, melting the lattice into a liquid. The mixed state is then separated into a solid at low temperatures and a liquid at high temperatures. The phase diagram for high- T_c superconductors is shown schematically in Fig. 1.6. The properties of the solid depend on the type and amount of disorder, which also determine the nature of the solid-to-liquid transition.

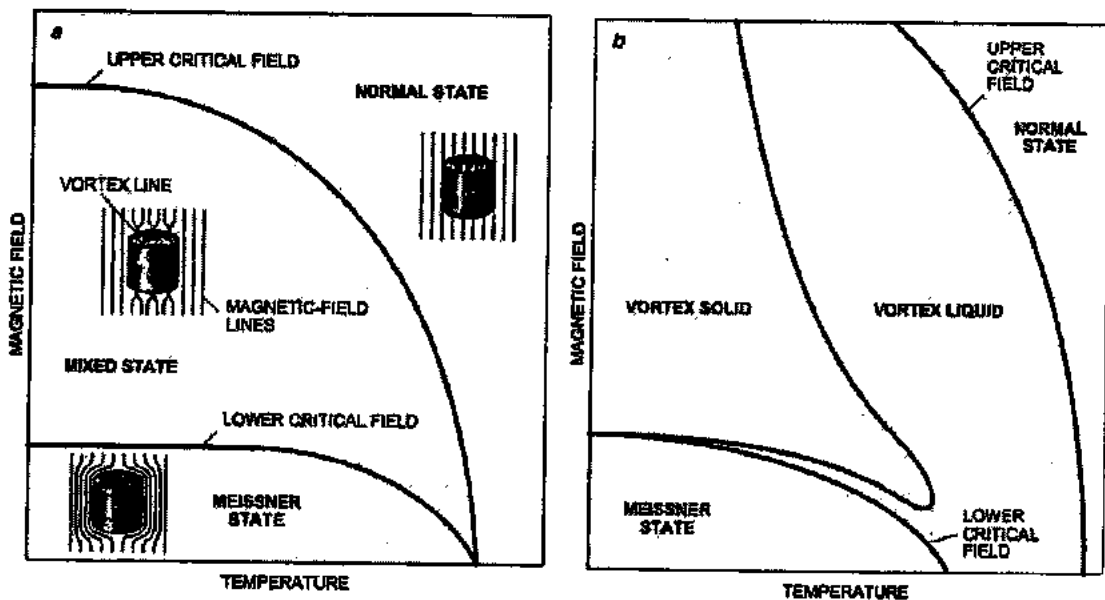


Fig. 1.6: The phase diagram show: (a) the type II superconductor under influence of external magnetic field and three phases present in a conventional superconductor. (b) Shows the HTSc with vortex liquid and vortex solid regimes [42].

1.4.4 Vortex liquid

The flux line lattice melts into a liquid at high temperatures or magnetic fields. In the vortex liquid state, the correlation between vortices is lost and they start moving around under the influence of thermal energy and Lorentz forces, which causes dissipation. The pinning in the liquid phase is not much effective as in the solid state due to the lack of correlation between vortices. Thus the liquid state always shows a non-zero resistivity, even for small current densities. At temperatures just below the melting transition the lattice becomes softer and a peak appears in j_c . Soft vortex matter can adapt better to the pinning landscape, explaining the appearance of the peak. This effect was observed by Kwok and their fellows at high temperature superconductors [43]. Just above the melting temperature the TAFF regime is entered. In this region pinning is still effective and the liquid is very viscous, with a resistivity smaller than in the flux flow regime. The reduced resistivity could be due to entanglement in the liquid [44].

The hydrodynamic theory proposed by Marchetti and Nelson, where the liquid state is described through a flux liquid viscosity, which is large due to the entanglement [45]. In TAFF regime the decreased in resistivity is observed due to strong pinning centers whose effect is transmitted over large distances. When the liquid is unpinned the flux flow regime is achieved at high temperature. The current dependence of the resistivity in the different regimes is schematically shown in Fig. 1.7.

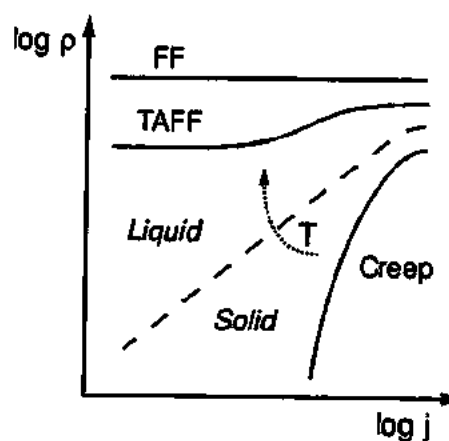


Fig.1.7: Schematic plot of resistivity ρ vs. current density j for a clean superconductor. At high temperatures the pinning barriers are much smaller than thermal energy and the system is in the flux flow regime (FF). As T decreases and the system gets closer to the solid phase, the pinning barriers become large compared to the thermal energy (TAFF regime). In the solid the resistivity comes from creep motion of the vortices [46].

In high temperature superconductors the magnetic relaxation processes are quick over a large region of the phase diagram below H_{c2} , leading to a reversible magnetization. This region is limited at low temperatures by the irreversibility line. This behavior of the magnetization was observed in 1987 in the Ba-La-Cu-O system [47]. They interpreted their observation as evidence of a superconducting glass state. Many researchers described the irreversibility line as a depinning line, using a thermally-activated flux-creep model [46, 48]. However, the origin of the irreversibility line has been a controversial issue and some researchers attribute it to the phase transition from the solid to the liquid [49], either melting or second-order glass transition [50].

1.4.5 Vortex solid

The comparison between the pinning energy and the elastic energy helped to determine properties of vortex solid. In defect landscape the vortices will try to accommodate while maintaining the lattice. In an ideal material with no pinning centers the solid state would be a perfect Abrikosov lattice. The distortions of the lattice is not important, if the density of defect is low in the material then the solid is a quasicrystal lattice or Bragg glass [51]. In vortex solid phase the Bragg diffraction peaks are observed and the translational long range order is preserved [52]. When the temperature reaches the melting temperature T_m , the system undergoes a first-order transition into the liquid state.

The pinning energy will prevail and solid phase cannot exist as a perfect lattice, if the pinning centers are strong or there is a large amount of them. In the presence of correlated disorder, like impurities or oxygen vacancies, the proposed model for solid state is known as vortex glass state [50].

This state also behaves as superconducting state: for small currents ($j \rightarrow 0$) where the pinning barriers become infinite, to prevent any kind of creep motion and making $\rho \rightarrow 0$. The transition between the vortex glass and the vortex liquid is second order transition, while the first order melting is observed in pure sample.

In the presence of correlated disorder, like the twin boundaries in YBCO are columnar defects is slightly different. The vortices are pinned by columnar defects did not show any angular dependence and anisotropy in the vortex glass region. When the

magnetic field is applied in parallel to the defects the solid is called Bose glass state and these systems are extensively studied by researcher [53, 54].

1.5 Aims and objectives of research

1. The main goal of this research is to improve infield superconducting properties especially critical transition temperature (T_c), upper critical field (H_{c2}) and inter-grain coupling by the introduction of artificial pinning centers after inclusion of metallic nanoparticles in CuTl-1223 matrix.
2. In order to attain highest critical transition temperature (T_c), upper critical field (H_{c2}) and to improve inter- grain coupling and superconducting volume fraction different types, concentrations and sizes of metallic nanoparticles will be added in CuTl-1223 superconducting matrix.
3. The experimental results will be analyzed on the basis of different established models and theories and will be compared with the previous findings by the different research groups working in this area.
4. This research work will guide us for the synthesis of superconducting materials with the enhanced superconducting properties, which is the demand of advance practical applications.

References

- [1] H. K. Onnes, "The resistance of pure mercury at helium temperatures" *Commun. Phys. Lab. Univ. Leiden.* **12** (1911) 1.
- [2] J. Bardeen, L. N. Cooper, and J. R. Schrieffer, "Microscopic theory of superconductivity" *Phys. Rev.* **106** (1957) 162.
- [3] J. Bardeen, L. N. Cooper, and J. R. Schrieffer, "Theory of superconductivity" *Phys. Rev.* **108** (1957) 1175.
- [4] I. Giaever, "Detection of the ac Josephson Effect" *Phys. Rev. Lett.* **14** (1965) 904.
- [5] B. D. Josephson, "Possible new effects in superconductive tunnelling" *Phys. Lett.* **1** (1962) 251.
- [6] H. Ibach, and H. Luth, "Solid-State Physics. An introduction to principles of materials science" Springer, (2009).
- [7] X. Xiaojun, F. Lan, W. Liangbin, Z. Yuheng, F. Jun, C. Xiaowen, L. Kebin, and S. Hisashi, "Dependence of activation energy upon magnetic field and temperature in $\text{YBa}_2\text{Cu}_3\text{O}_{7-\delta}$ epitaxial thin film" *Phys. Rev. B* **59**, (1999) 608.
- [8] Fossheim, Kristian. "Superconductivity: Discoveries and Discoverers." Springer-Verlag Berlin Heidelberg (2013).
- [9] J. Bardeen, L. N. Cooper, and J. R. Schrieffer, "Theory of superconductivity" *Phys. Rev.* **108**, (1957) 1175.
- [10] B. Rosenstein, and D. Li, "Ginzburg-Landau theory of type II superconductors in magnetic field" *Revi. Phys.* **82** (2010) 109.
- [11] I. Zutic, J. Fabian, and S. D. Sarma, "Spintronics: Fundamentals and applications" *Rev. Phys.* **76** (2004) 323.
- [12] L. Testardi, J. Wernick, and W. Royer, "Superconductivity with onset above 23° K in Nb Ge sputtered films" *Solid State Comm.* **15** (1974) 1.
- [13] J. Gavaler, "Superconductivity in Nb-Ge films above 22 K" *App. Phys. Lett.* **23** (1973) 480.
- [14] J. G. Bednorz, and K. A. Müller, "Possible high T_c superconductivity in the Ba-La-Cu-O system" *Phys. B* **64** (1986) 189.
- [15] M. K. Wu, J. R. Ashburn, C. J. Torng, P. H. Hor, R. L. Meng, L. Gao, Z. J. Huang, Y. Wang, and C. Chu, "Superconductivity at 93 K in a new mixed-phase Y-Ba-Cu-O compound system at ambient pressure" *Phys. Rev. Lett.* **58** (1987) 908.
- [16] Z. Zhao, L. Chen, Q. Yang, Y. Huang, G. Chen, R. Tang, G. Liu, Y. Ni, C. Cui, and L. Chen, "Superconductivity above liquid nitrogen temperature in new oxide systems" *Kexue Tongbao.* **32** (1987) 1098.
- [17] T. VanDuzer, and W. V. Hassenzahl, "Scanning the issue-special issue on applications of superconductivity" *IEEE.* **92** (2004) 1511.
- [18] L. Civale, B. Maiorov, A. Serquis, J. Willis, J. Coulter, H. Wang, Q. Jia, P. Arendt, J. a. MacManus-Driscoll, and M. Maley, "Angular-dependent vortex pinning mechanisms in $\text{YBa}_2\text{Cu}_3\text{O}_7$ coated conductors and thin films" *Appl. Phys. Lett.* **84** (2004) 2121.
- [19] R. Griessen, W. Hai-Hu, A. Van Dalen, B. Dam, J. Rector, H. Schnack, S. Libbrecht, E. Osquiguil, and Y. Bruynseraede, "Evidence for mean free path fluctuation induced pinning in $\text{YBa}_2\text{Cu}_3\text{O}_7$ and $\text{YBa}_2\text{Cu}_4\text{O}_8$ films" *Phys. Rev. Lett.* **72** (1994) 1910.
- [21] P. C. McIntyre, M. J. Cima, J. A. Smith Jr, R. B. Hallock, M. P. Siegal, and J. M. Phillips, "Effect of growth conditions on the properties and morphology of chemically derived epitaxial thin films of $\text{Ba}_2\text{YCu}_3\text{O}_{7-x}$ on (001) LaAlO_3 " *J. Appl. Phys.* **71** (1992) 1868.

- [22] T. Araki, and I. Hirabayashi, "Review of a chemical approach to $\text{YBa}_2\text{Cu}_3\text{O}_{7-x}$ coated superconductors metalorganic deposition using trifluoroacetates" *Supercond. Sci. Technol.* **16**, (2003) 71.
- [23] M. Liu, H. Suo, S. Ye, D. Shi, Y. Zhao, X. Tang, L. Ma, Q. Li, L. Wang, and M. Zhou, "Preparation and properties of YSZ-doped YBCO films grown by the TFA-MOD method" *Supercond. Sci. Technol.* **21** (2008) 115012.
- [24] H. Ihara, K. Tanaka, Y. Tanaka, A. Iyo, N. Terada, M. Tokumoto, M. Ariyama, I. Hase, A. Sundaresan, and N. Hamada, "Mechanism of T_c enhancement in $\text{Cu}_{1-x}\text{Tl}_x\text{-1234}$ and-1223 system with $T_c > 130$ K" *Physica C* **341** (2000) 487.
- [25] N. Stavitski, V. Lyahovitskaya, J. Nair, J. ZON, R. Popovitz-Biro, E. Wachtel, Y. Feldman, and I. Lubomirsky, "Substrate-free crystallization of distorted hexagonal barium titanate thin films" *App. Phys. Lett.* **81** (2002) 4177.
- [26] D. Tenne, X. Xi, Y. Li, L. Chen, A. Soukiassian, M. Zhu, A. James, J. Lettieri, D. Schlom, and W. Tian, "Absence of low-temperature phase transitions in epitaxial BaTiO_3 thin films" *Phys. Rev. B* **69** (2004) 174101.
- [27] W.-S. Cho, E. Hamada, and K. Takayanagi, "Stacking faults in BaTiO_3 particles synthesized from organic precursor" *J. Appl. Phys.* **81** (1997) 3000.
- [28] M. R. Mohammadi, A. E. Rad, and D. Fray, "Water-based sol-gel nanocrystalline barium titanate: controlling the crystal structure and phase transformation by Ba:Ti atomic ratio" *J. Mater. Sci.* **44** (2009) 4959.
- [29] A. K. Jha, and N. Khare, "Strongly enhanced pinning force density in YBCO- BaTiO_3 nanocomposite superconductor" *Physica C* **469** (2009) 810.
- [30] M. Mumtaz, S. Hasnain, A. Khurram, and N. A. Khan, "Fluctuation induced conductivity in $(\text{Cu}_{0.5}\text{Tl}_{0.5-x}\text{K}_x)\text{Ba}_2\text{Ca}_3\text{Cu}_4\text{O}_{12-8}$ superconductor" *J. Appl. Phys.* **109** (2011) 023906.
- [31] M. Mumtaz, S. Hasnain, A. Khurram, and Nawazish. A. Khan, "Fluctuation induced conductivity in $(\text{Cu}_{0.5}\text{Tl}_{0.5-x}\text{K}_x)\text{Ba}_2\text{Ca}_3\text{Cu}_4\text{O}_{12-8}$ superconductor" *J. Appl. Phys.* **109**, (2011) 023906.
- [32] R. Awad, "Enhancement the formation of (Cu, Tl)-1223 superconducting phase by Cd-substitution" *J. Alloys Compd.* **474** (2009) 517.
- [33] A. A. Abrikosov, "On the magnetic properties of superconductors of the second group" *Sov. Phys. JETP* **5** (1957) 1174.
- [34] U. Essmann, and H. Trauble, "The direct observation of individual flux lines in type II superconductors" *Phys. Lett. A* **24** (1967) 526.
- [35] P. Gammel, D. Bishop, G. Dolan, J. Kwo, C. Murray, L. Schneemeyer, and J. Waszczak, "Observation of hexagonally correlated flux quanta in $\text{YBa}_2\text{Cu}_3\text{O}_7$ " *Phys. Rev. Lett.* **59** (1987) 2592.
- [36] A. Moser, H. Hug, I. Parashikov, B. Stiefel, O. Fritz, H. Thomas, A. Baratoff, H. J. Güntherodt, and P. Chaudhari, "Observation of single vortices condensed into a vortex-glass phase by magnetic force microscopy" *Phys. Rev. Lett.* **74** (1995) 1847.
- [37]] P. E. Goa, H. Hauglin, M. Baziljevich, E. Ilyashenko, P. L. Gammel, and T. H. Johansen, "Real-time magneto-optical imaging of vortices in superconducting NbSe_2 " *Supercond. Sci. Technol.* **14** (2001) 729.
- [38] A. Larkin, and Y. N. Ovchinnikov, "Pinning in type II superconductors" *J. Low Temp. Phys.* **34** (1979) 409.
- [39] P. W. Anderson, "Theory of flux creep in hard superconductors" *Phys. Rev. Lett.* **9** (1962) 309.
- [40] P.W. Anderson, and Y.B. Kim, , "Hard superconductivity: theory of the motion of Abrikosov flux lines" *Rev. Mod. Phys.* **36**, (1964) 39.

- [41] D. Dew-Hughes, "Model for flux creep in high T_c superconductors" *Cryogenics* **28**, (1988) 674.
- [42] D. J. Bishop, P. L. Gammel, and D. A. Huse, "Resistance in high-temperature superconductors" *Sci. Am.* **268** (1993).
- [43] W. Kwok, J. Fendrich, C. Van der Beek, and G. Crabtree, "Peak effect as a precursor to vortex lattice melting in single crystal $\text{YBa}_2\text{Cu}_3\text{O}_{7-\delta}$ " *Phys. Rev. Lett.* **73**, (1994) 2614.
- [44] D. R. Nelson, and H. S. Seung, "Theory of melted flux liquids" *Phys. Rev. B* **39**, (1989) 9153.
- [45] M. C. Marchetti, and D. R. Nelson, "Hydrodynamics of flux liquids" *Phys. Rev. B* **42**, (1990) 9938.
- [46] G. Fuchs, K. Nenkov, A. Attenberger, K. Lüders, M. Baenitz, C. Ecker, K. Kajikawa, E. Antipov, and H. Khan, "A uniform description of irreversibility lines for various high- T_c superconductors" *Physica C* **355** (2001) 299.
- [47] K. Müller, M. Takashige, and J. Bednorz, "Flux trapping and superconductive glass state in $\text{La}_2\text{CuO}_{4-y}\text{:Ba}$ " *Phys. Rev. Lett.* **58**, (1987) 1143.
- [48] T. Matsushita, "On the origin of the irreversibility line in superconductors Depinning or melting of fluxoids" *Physica C* **214** (1993) 100.
- [49] A. Schilling, M. Cantoni, J. Guo, and H. Ott, "Superconductivity above 130 K in the Hg-Ba-Ca-Cu-O system" *Nature* **363** (1993) 56.
- [50] M. P. Fisher, "Vortex-glass superconductivity: a possible new phase in bulk high- T_c oxides" *Phys. Rev. Lett.* **62** (1989) 1415.
- [51] T. Giamarchi, and P. Le Doussal, "Phase diagrams of flux lattices with disorder" *Phys. Rev. B* **55** (1997) 6577.
- [52] T. Klein, I. Joumard, S. Blanchard, J. Marcus, R. Cubitt, T. Giamarchi, and P. Le Doussal, "A Bragg glass phase in the vortex lattice of a type II superconductor" *Nature* **413** (2001) 404.
- [53] A. Larkin, and V. Vinokur, "Bose and vortex glasses in high temperature superconductors" *Phys. Rev. Lett.* **75** (1995) 4666.
- [54] D. R. Nelson, and V. Vinokur, "Boson localization and correlated pinning of superconducting vortex arrays" *Phys. Rev. B* **48** (1993) 13060.

Chapter 2: Thermally Assisted Flux Flow and Literature Review

2.1 Thermally assisted flux flow (TAFF)

When applied current is low, some superconductors of type II show an ohmic response even at low temperature under the applied magnetic field. In this case, the pinning barriers are larger as compared to thermal energy, but still finite and the system acts as a very viscous liquid proposed the thermally assisted flux flow (TAFF) model to describe physics of this region [1]. The ohmic response can also be calculated from Eq. 1.7 as for small currents are possible to linearize $\sinh(x) \sim x$ and obtaining a resistivity, which is also known as Arrhenius equation.

$$\rho = \rho_0 e^{-U_0/k_B T} \dots\dots\dots 2.1$$

where ρ_0 is normal state resistivity and U_0 is activation energy, these are field and temperature dependent. The general form suggested for the dependence of U_0 near T_c is

$$U_0 \propto (1-t)^q B^{-\beta} \dots\dots\dots 2.2$$

where t is reduced temperature and $t = T/T_c$. The exponent q has the value between 1 to 1.5 [2] and this value is in agreement with the theory of a pinned vortex liquid developed by Geshkenbein and Vinokur [3-4]. The exponent β depends on the anisotropy of the material and also on magnetic field [5]. At low current densities, U_0 is current independent, while at high currents follows $U_0 \propto \ln(j_c/j)$.

According to Eq. 2.1, the resistivity should obey $\ln \rho \propto 1/T$. In an Arrhenius plot of $\ln \rho$ versus $1/T$, the TAFF regime corresponds to the linear low resistance part as shown in Fig. 2.1. At higher temperatures and resistances, the flux flow regime is entered.

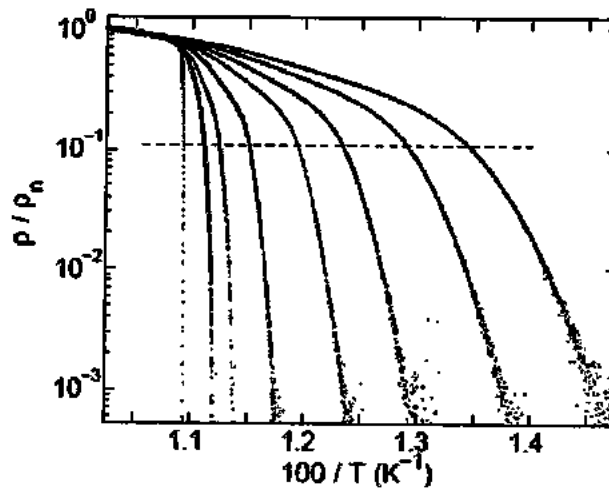


Fig. 2.1: Arrhenius plot of normalized resistance for the YBCO single crystal, in magnetic fields $B \parallel c$ at 0, 0.5, 1, 2, 4, 6, 9 and 12 T (left to right). The dashed line marks the crossover from flux flow at high temperatures to TAFF at low resistivity [6].

2.2 Effect of nanostructures inclusion in HTSCs

Ansari *et al.* [7] investigated magneto-resistivity of diamond doped MgB_2 superconductor at different magnetic fields. They revealed that the $U_o(B)$ behave as a nonlinear function of current density $U_o \propto J_c^{-0.2}$. The $U_o(B)$ of diamond doped MgB_2 was determined and found to be decreased with associated applied field. At high field range about 8 T, 5 % diamond doped MgB_2 showed the highest activation energy $\{U_o(B)\}$ as compared to other samples. The results also revealed that the activation energy shows a decreasing trend with increasing magnetic field. The irreversibility (H_{ir}) was increased by doping the diamond and 5 % doped MgB_2 showed the more irreversibility as compared to others samples. The current density decreased rapidly as the applied field increased, the value of activation energy is also lower.

Khurram *et al.* [8] studied the energy dissipation in $Tl_{1-x}C_xBa_2Ca_3Cu_4O_{12.8}$ ($x = 0, 0.25, 0.5$ and 0.75) superconductor in presence of external magnetic field. With $x = 0.25$ carbon content, the sample has strong flux pinning ability. The higher carbon content has poor grains morphology and has weak flux pinning ability. The resistive transition bordering was fitted according to thermally activated flux flow (TAFF) model. They used Arrhenius plot and take the region close to $T_c(0)$ to determine the activation energy (U_o).

Zouaoui *et al.* [9] reported magneto-resistivity of $(Bi,Pb)_2Sr_2Cu_3O_x$ with the addition of Al_2O_3 nano-particles with 0 and 0.2 wt. % ratios. Magneto-resistivity and

the energy dissipation phenomenon were analyzed and compared by using the thermally assisted flux creep (TAFC) model. The effective U_0 was enhanced with 0.2 wt. % addition of Al_2O_3 nano-particles as compared to free one. Vortex phase diagram showed characteristic of T_g and T_p which was increased with the addition Al_2O_3 with 0.2 wt. %.

Vinu *et al.* [10] investigated the resistivity of $Bi_{1.6}Pb_{0.5}Sr_{2-x}Eu_xCa_{1.1}Cu_{2.1}O_{8-x}$ ($0.0 \leq x \leq 0.180$) under the influence of magnetic field and temperature. The resistivity showed a glassy behavior at high temperature and applied magnetic field in Eu doped samples. The value of critical temperature T_c was gradually increased up to $x = 0.180$. But the value of glass transition temperature T_g and $U_0(T,B)$ were found maximum for $x = 0.135$. At high temperature and magnetic field the vortices lines were effectively pinned. The scaling analysis was also valid for vortex-liquid system for Eu-doped (Bi, Pb)-2212 samples.

Ghorbani *et al.* [11] investigated the vortex in mixed state for $Ba_{0.72}K_{0.28}Fe_2As_2$ (BK-122), $Ba(Fe_{0.95}Ni_{0.05})_2As_2$ (BaNi-122) and $Ba(Fe_{0.91}Co_{0.09})_2As_2$ (BaCo-122) single crystal having the critical temperatures $T_c = 31.7$ K, 18 K and 17.3 K respectively. The results showed that the vortex state is 3-D at lower temperature than a characteristic temperature (T^*). Vortex phase diagram was obtained, which was based on the glass transition temperature (T_g) and the upper critical field H_{c2} . It is also observed that non-magnetic K doping causes a high glass line close to the H_{c2} , while the magnetic doping of Ni and Co result a low glass line, which was far away from H_{c2} . They suggested that non-magnetic induced disorder was more favorable for the improvement of pinning strength as compared to magnetic induced disorder. They also showed that the pinning potential was responsible for difference in glassy states.

Awad *et al.* [12] investigated the magnetoresistivity of superconductor $TlBa_2Ca_{2-x}Sc_xCu_3O_{9.5}$ ($x = 0, 0.025, 0.05, 0.1$ and 0.2); which was prepared by solid-state reaction. The flux motion had been investigated at low magnetic field on electrical resistivity of samples. At high magnetic field there was a slightly change in T_c and transition broadening ΔT . Arrhenius relation was used to calculate the pinning energy $U_0(B)$, it increased in $x = 0.05$ and decreased for other concentrations. The magnetic field dependent activation energy $U_0(B)$ followed the power law. The

activation energy $U_0(B,T)$ was found as $U(B,T) \sim \Delta T B^{-\eta}$, where $\eta = \beta + n$. Wiedemann-Franz law was used to calculate the electronic thermal conductivity κ_e .

Zhang *et al.* [13] synthesized Al doped Bi-2212 bulk superconductor by using spark plasma sintering (SPS). The particle size of Al nanoparticles was in 5-30 nm, which work as effective pinning centers to increase the flux pinning ability of Bi-2212. The influence of Al doping on microstructures, transport and superconducting properties, include flux pinning properties have been investigated. With the doping of Al nanoparticles in Bi-2212 bulks under applied magnetic field was improved by both increase in activation energy and improve in flux pinning force. The activation energy and flux pinning force enhanced after the doping of Al nanoparticles, which was evidence for the enhancement of pinning mechanism. This work provided a path to introduce the flux pinning centers in Bi-2212 system to increase its current capacity.

Sharma *et al.* [14] investigated the magnetoresistivity of $\text{Bi}_2\text{Sr}_2\text{CaCu}_2\text{O}_{8+\delta}$ and calculated the transition width by this relation $T_c^{\text{onset}} - T_c^{R=0}$. The critical temperature $T_c(0)$ was enhanced from 32 K to 82 K by increasing the sintering temperature which improved the grain morphology. The resistive transition broadening ΔT was increased by decreasing the sintering temperature and T_c^{onset} didn't affect the grain morphology. Activation energy (U_0) and ΔT was also analyzed in the presence of magnetic field, which was explained by TAFF model and it was found that magnetic field dependence activation energy obey the power law. It clearly observed that the grain morphology (flux pinning) played a vital role in the TAFF resistive broadening. For feasible application, HTS Bi-2212 compounds were needed to synthesize at their melting point, to obtain the better inter-grain connectivity.

Vinu *et al.* [15] was investigated, the vortex glass resistivity in the mixed sate region by Ho doped (Bi,Pb)-2112 superconductor. Due to thermal fluctuations in vortex, a large resistive transition broadening was observed in applied magnetic field. Activation energy $U_0(T,B)$ was calculated by vortex glass to liquid transition theory. At high magnetic field and temperature the resistivity showed a glass behavior for $x = 0.075$, which was due to point defect created by doped Ho nanoparticles in (Bi, Pb)-2212 matrix. The value of T_g , Activation energy $U_0(T,B)$ and magnetic field dependent activation energy $U_0(B)$ were founded maximum for $x = 0.075$, which clearly showed that the flux lines were strongly pinned. The increase in

superconducting transition temperature T_c , glass transition temperature T_g and the activation energy $U_0(T, B)$ were due to doping of Ho in (Bi, Pb)-2212 system, which had scientific and technological significance to understand the behavior of vortex in HTSC.

Nazarova *et al.* [16] analyzed the effect of external field on different properties of pure and Ag doped superconductor $\text{FeSe}_{0.94}$. It was observed that the doping of Ag nanoparticles in $\text{FeSe}_{0.94}$ suppressed the hexagonal phase formation and strongly enhanced the grain connectivity. The superconducting transition temperature T_c and the upper critical field H_{c2} were increased; where as normal state resistivity was reduced, which was comparable with the FeSe single crystals. The resistive transition broadening of pure and Ag doped in $\text{FeSe}_{0.94}$ was analyzed by using the TAFF model. The activation energy U_0 calculated by TAFF model was related to sharp superconducting transition of Ag doped $\text{FeSe}_{0.94}$. It was also observed that Ag doping improve the magnetoresistance and upper critical field H_{c2} . The magnetic field dependent activation energy $U_0(H)$ showed the collective creep pinning behavior with increasing magnetic field.

Yildirim *et al.* [17] investigated the anisotropic behavior of Bi-2212 superconductor thin film under the external magnetic field. The magnetoresistivity versus temperature curves were used to deduce the transition temperature (T_c), irreversibility field ($\mu_0 H_{irr}$) and upper critical field (H_{c2}). The activation energy U_0 was calculated by using the thermally activated flux flow (TAFF) model. It was observed that when the magnetic field was perpendicular to c-axis the value of T_c shifted from 76.4 K to 39.1 K; similarly when applied magnetic field was parallel to c-axis the T_c reduced to 28.8 K. Furthermore the values of activation energy U_0 were decreased with increasing the magnetic field, the smallest value of U_0 was obtained when the applied field was parallel to c-axis. The values of $\mu_0 H_{irr}$ and $\mu_0 H_{c2}$ were found to be decreased with the increasing the applied magnetic field. The values of coherence lengths (ξ) and penetration depths (λ) inferred from $\mu_0 H_{irr}(0)$ and $\mu_0 H_{c2}(0)$ were found to be increased when the applied magnetic field was parallel to c-axis.

Dadras *et al.* [18] investigated the effect of (CNTs) on crystal structure and superconducting properties of (Y-123) compound. I-V measurements in presence of magnetic field were used to analyze the pinning energy U_j and critical current density

J_c , as a function of applied magnetic field at fixed temperature. The addition of CNTs didn't change the superconducting transition temperature T_c , it remained 91-92 K. The addition of CNTs contents up to 0.7 wt. % enhanced both the pinning energy U_j and the critical current density J_c , while the J_c was ten times greater in 0.7 wt. % CNT than pure sample. The SEM images showed that the doping of CNT enhanced the electrical conductivity between the grains as a result J_c was increased.

Liu *et al.* [19] investigated the resistive transition broadening along c-axis in $\text{La}_{1.6-x}\text{Nd}_{0.4-x}\text{Sr}_x\text{CuO}_4$ epitaxial films ($x = 0.1, 0.12, 0.14$ and 0.16) under the influence of applied magnetic field. For H \parallel c, the field dependent activation energy was based on power law i.e., $\{U_0(H) \propto H^\alpha (\alpha \sim 1)\}$. For H \parallel c, the flux pinning centers were formed as a result of dislocations and grain boundary. It was also observed that in-plane or tails of resistivity below mean field transition temperature $T_c(H)$ was based on Arrhenius type thermally activated flux flow (TAFF) model. For H \perp c, a logarithmic dependence of activation energy was analyzed due to intrinsic pinning in high T_c superconductors, which played a vital role to determine the behavior of the plastic creep.

References

- [1] P. Kes, J. Aarts, J. Van den Berg, C. Van der Beek, and J. Mydosh, "Thermally assisted flux flow at small driving forces" *Supercond. Sci. Technol.* **1** (1989) 242.
- [2] Y. Yeshurun, and A. Malozemoff, "Giant flux creep and irreversibility in an Y-Ba-Cu-O crystal: an alternative to the superconducting-glass model" *Phys. Rev. Lett.* **60** (1988) 2202.
- [3] Y. Abulafia, A. Shaulov, Y. Wolfus, R. Prozorov, L. Burlachkov, Y. Yeshurun, D. M. E. Zeldov, H. Wühl, V. Geshkenbein, and V. Vinokur, "Plastic vortex-creep in $\text{YBa}_2\text{Cu}_3\text{O}_{7-x}$ crystals" *Phys. Rev. Lett.* **77** (1996) 8.
- [4] X. Xiaojun, F. Lan, W. Liangbin, Z. Yuheng, F. Jun, C. Xiaowen, L. Kebin, and S. Hisashi, "Dependence of activation energy upon magnetic field and temperature in $\text{YBa}_2\text{Cu}_3\text{O}_{7-\delta}$ epitaxial thin film" *Phys. Rev. B* **59** (1999) 608.
- [5] T. Palstra, B. Batlogg, R. Van Dover, L. Schneemeyer, and J. Waszczak, "Critical currents and thermally activated flux motion in high-temperature superconductors" *Appl. Phys. Lett.* **54** (1989) 763.
- [6] B. Espinosa-Arronte, M. Djupmyr, and M. Andersson, "Scaling of the B-dependent resistivity for different orientations in Fe doped $\text{YBa}_2\text{Cu}_3\text{O}_{7-\delta}$ " *Physica C* **423** (2005) 69.
- [7] I. A. Ansari, M. Shahabuddin, N. S. Alzayed, A. Vajpayee, V. Awana, and H. Kishan, "Enhancement of activation energy in nano diamond doped MgB_2 superconductor" *Physica C* **470** (2010) 369.
- [8] A. Khurram, S. Ahmad, and Nawazish. A. Khan, "Flux pinning in $\text{Tl}_{1-x}\text{C}_x\text{Ba}_2\text{Ca}_3\text{Cu}_4\text{O}_{12-\delta}$ superconductor" *Physica C* **480** (2012) 19.
- [9] M. Zouaoui, A. Ghattas, M. Annabi, F. Ben Azzouz, and M. Ben Salem, "Magneto-resistance analysis of nanometer Al_2O_3 added Bi-2223 polycrystalline superconductors" *J. Phys.* **150** (2009) 052292.
- [10] S. Vinu, P. M. Sarun, R. Shabna, and U. Syamaprasad, "Analysis of thermomagnetic fluctuations above the glass-transition temperature in $\text{Bi}_{1.6}\text{Pb}_{0.5}\text{Sr}_{2-x}\text{Eu}_x\text{Ca}_{1.1}\text{Cu}_{2.1}\text{O}_{8+\delta}$ ($0.000 \leq x \leq 0.180$) system" *Solid State Sci.* **11** (2009) 1530.
- [11] S. R. Ghorbani, X. Wang, M. Shabazi, S. Dou, K. Choi, and C. Lin, "Flux pinning and vortex transitions in doped BaFe_2As_2 single crystals" *Appl. Phys. Lett.* **100** (2012) 072603.

- [12] R. Awad, I. H. Ibrahim, E. M. E. Mansour, M. Roumie, and A. Zein, "Magnetoresistance studies of Tl-1223 phase substituted by scandium" *J. Phys.* **97** (2008) 012323.
- [13] S. Zhang, M. Liang, C. Li, Q. Hao, J. Feng, and P. Zhang, "Enhanced flux pinning properties in Bi-2212 High temperature superconductors with nano-sized precipitates" *Mater. Lett.* **157** (2015)197.
- [14] D. Sharma, R. Kumar, and V. Awana, "Temperature and field dependence of thermally activated flux flow resistance in $\text{Bi}_2\text{Sr}_2\text{CaCu}_2\text{O}_{8+\delta}$ superconductor" *Solid State Comm.* **152** (2012) 941.
- [15] S. Vinu, P. Sarun, R. Shabna, A. Biju, and U. Syamaprasad, "Scaling of the vortex-liquid resistivity and temperature and magnetic field dependent activation energy in Ho doped (Bi, Pb)-2212 superconductor" *J. Appl. Phys.* **105** (2009) 123901.
- [16] E. Nazarova, N. Balchev, K. Nenkov, K. Buchkov, D. Kovacheva, A. Zahariev, and G. Fuchs, "Transport and pinning properties of Ag-doped $\text{FeSe}_{0.94}$ " *Supercond. Sci. Technol.* **28** (2015) 025013.
- [17] G. Yildirim, S. Bal, and A. Varilci, "Effect of Magnetic Field Direction on Magnetoresistivity, Activation Energy, Irreversibility and Upper Critical Field of Bi-2212 Thin Film Fabricated by DC Sputtering Method" *J. Supercond. Novel Magn.* **25** (2012) 1665.
- [18] S. Dadras, Y. Liu, Y. Chai, V. Daadmehr, and K. Kim, "Increase of critical current density with doping carbon nano-tubes in $\text{YBa}_2\text{Cu}_3\text{O}_{7-\delta}$ " *Physica C* **469** (2009) 55.
- [19] Y. Liu, and X. Li, "Irreversibility line and thermally activated flux flow in $\text{La}_{1.6-x}\text{Nd}_{0.4}\text{Sr}_x\text{CuO}_4$ films" *J. Appl. Phys.* **99** (2006) 3903.

Chapter 3: Synthesis and Characterization Techniques

3.1 Nanoparticles synthesis

Nanoparticles have been synthesized by two different approaches. One is the physical (top down approach) and other is chemical (bottom up approach). In physical method, bulk materials are reduced, subtract or subdivide to obtain nanoparticles in huge amount but with the distribution of broad size of obtaining nanoparticles. In chemical method atoms, ions or molecules are nucleating each other to get required nanoparticles, whose size can be controlled according to the desire. The advantage of chemical method is that the particles of the same size and chemical composition can be reproduced [1]. The systematic diagram of two approaches is shown in Fig. 3.1.

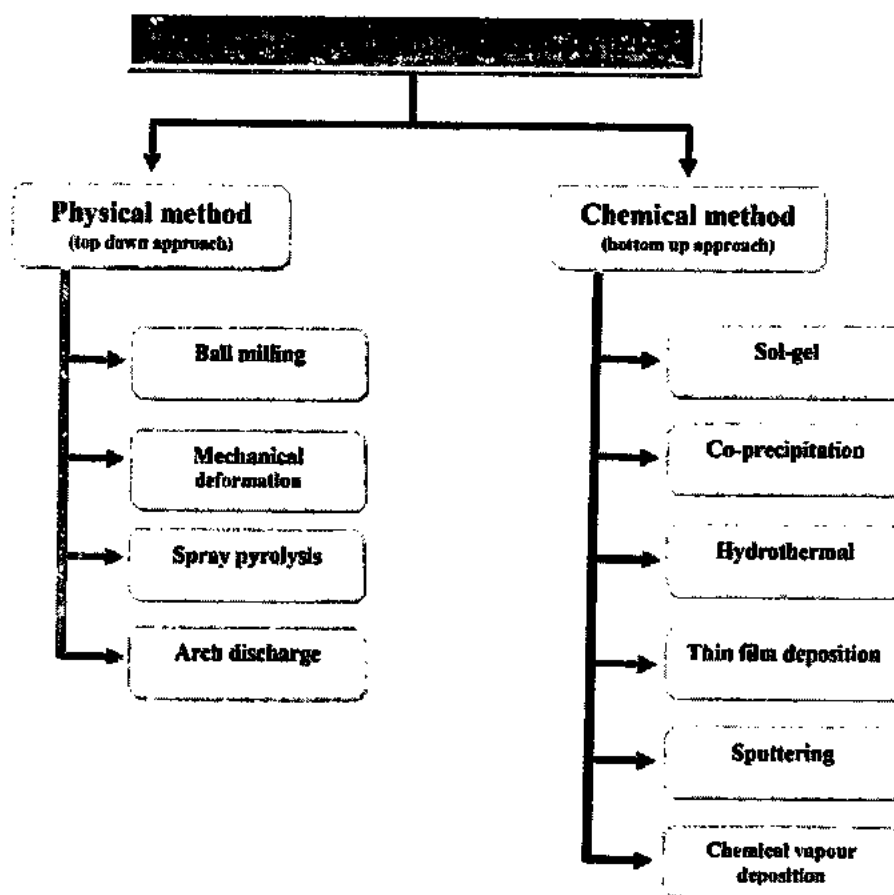


Fig. 3.1: Systematic diagram of physical and chemical methods for nanoparticles synthesis.

3.1.1 Ag nanoparticles synthesis

We used Sol gel method to synthesize Ag nanoparticles. For this purpose, we make the solution of silver nitrate and citric acid separately with distilled water. Then

stirred the mixture of two solutions and maintained the pH up to 5 with drop by drop addition of ammonia. The schematic diagram of preparation of Ag nanoparticles is shown in Fig. 3.2.

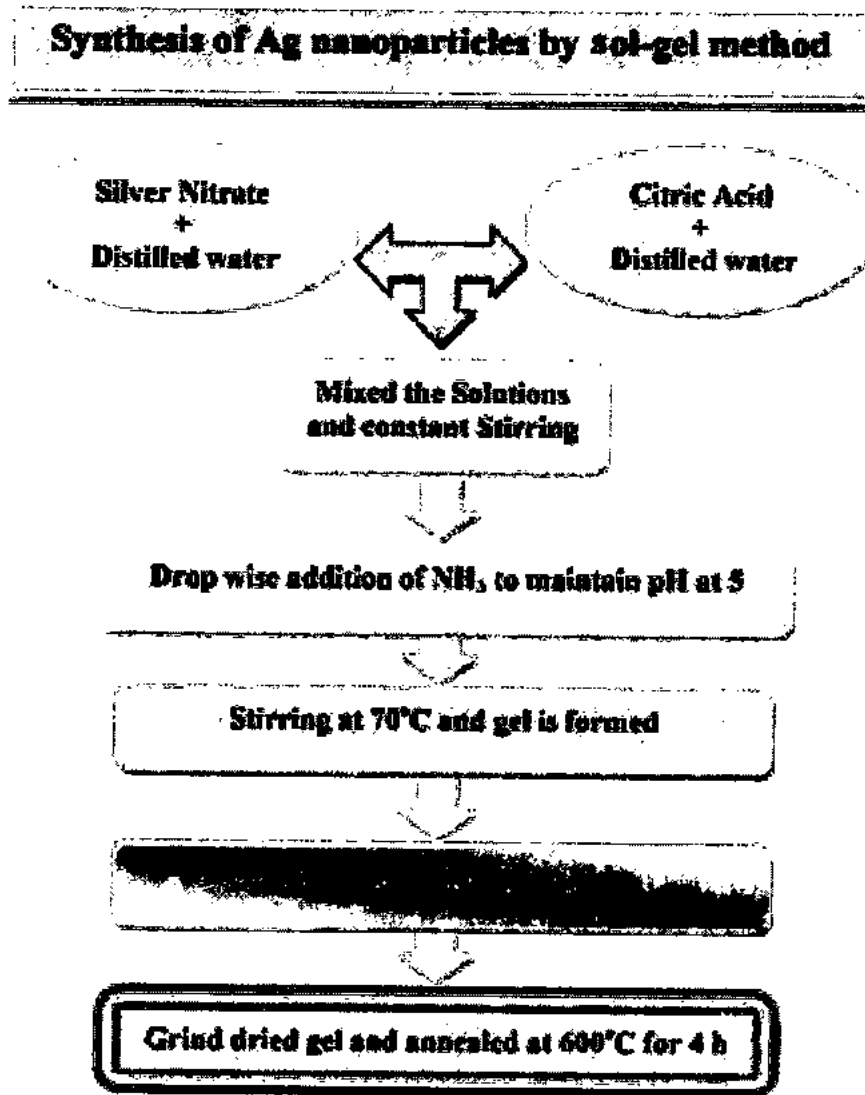


Fig. 3.2: Flow chart of Ag nanoparticle synthesis.

After adjusting pH at 5, we start heating at 70°C with constant stirring. The solution is converted into gel after 15 minutes. We stop stirring and placed the gel into oven at 110°C for 12 hours for drying gel. We ground the dry gel to get fine powder and annealed at 600°C for 4 hours. After grinding and annealing, we got Ag nanoparticles.

3.1.2 Synthesis of $\text{Cu}_{0.5}\text{Ba}_2\text{Ca}_2\text{Cu}_3\text{O}_{10-\delta}$ precursor

The synthesis of CuTl-1223 ($\text{Cu}_{1-x}\text{Tl}_x\text{Ba}_2\text{Ca}_2\text{Cu}_3\text{O}_{10-\delta}$) superconductor matrix was done by solid state reaction. First of all we took three compounds $\text{Cu}_2(\text{CN})_2 \cdot \text{H}_2\text{O}$, $\text{Ca}(\text{NO}_3)_2$ and $\text{Ba}(\text{NO}_3)_2$ in appropriate ratios. First of all, we mixed these compounds and ground for two hours in agate mortar and pestle. Then we loaded in quartz boats and placed in furnace for 12 hours at 860°C . After 12 hours, we switched off the furnace and wait until the furnace reached at room temperature. The sample was ground for two hours again and loaded in ceramic boats for heating at 860°C in order to get the final precursor. The schematic chart for synthesis of $\text{Cu}_{0.5}\text{Ba}_2\text{Ca}_2\text{Cu}_3\text{O}_{10-\delta}$ precursor is shown in Fig. 3.3.

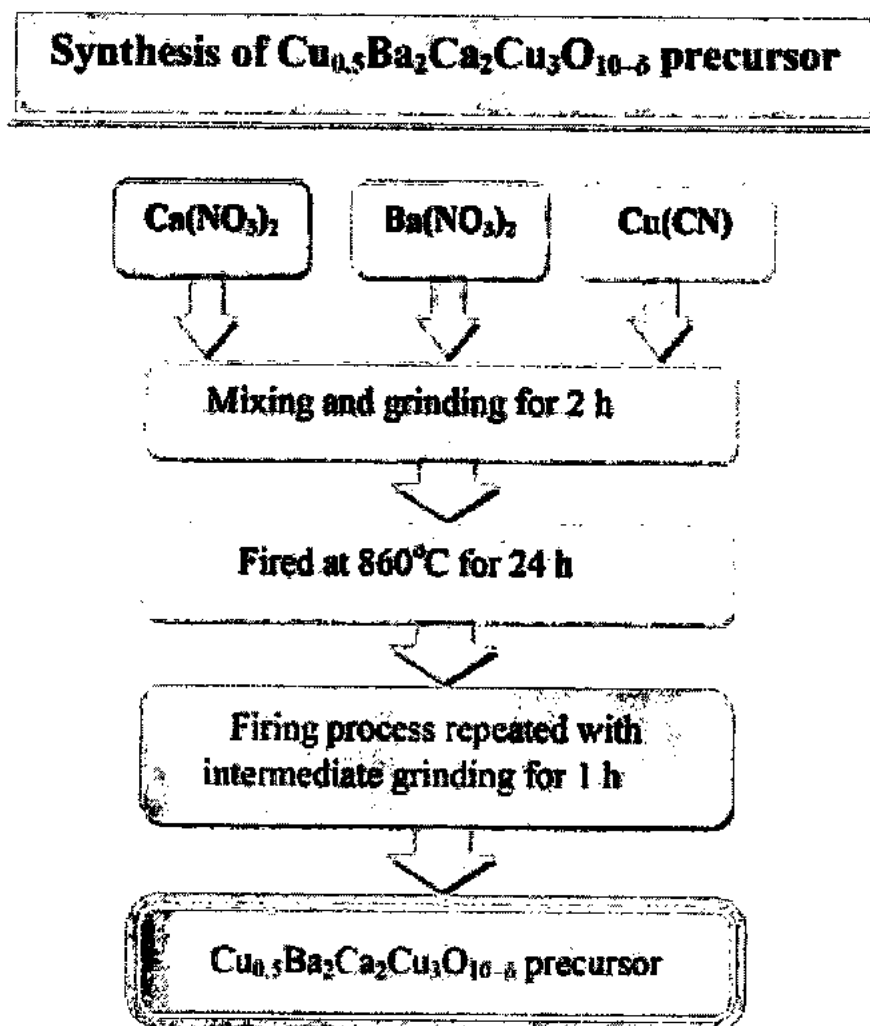


Fig. 3.3: Schematic flow chart of synthesis of $\text{Cu}_{0.5}\text{Ba}_2\text{Ca}_2\text{Cu}_3\text{O}_{10-\delta}$ precursor.

3.1.3 Synthesis of $(Ag)_x/CuTl-1223$ nanoparticles superconductor composite

We synthesized the Ag nanoparticles and $Cu_{0.5}Ba_2Ca_2Cu_3O_{10-\delta}$ precursor separately. Then we mixed Thallium oxide Tl_2O_3 and Ag nanoparticles with different concentrations ($x = 0, 0.5, 1.0, 1.5, 2.0$ and 4.0 wt. %) in precursor material. We ground this material for two hours, and pelletized with help of hydraulic press, and then placed the pellets in the gold capsules and sintered at $860^\circ C$ for 10 minutes one by one. By using this procedure, we synthesized the $(Ag)_x/CuTl-1223$ nanoparticles superconductor composite.

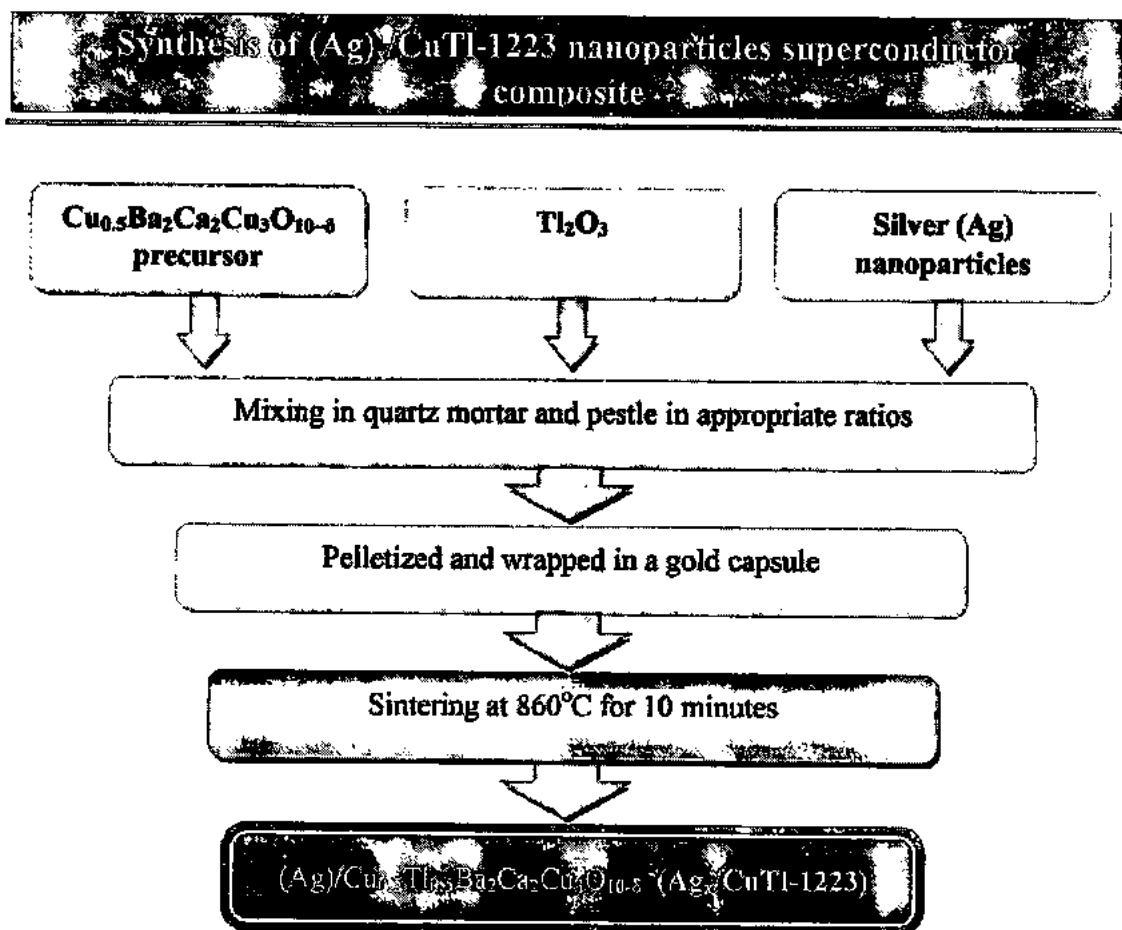


Fig. 3.4: Schematic diagram of $(Ag)_x/CuTl-1223$ nanoparticles superconductor composite.

3.2 Characterization Techniques

We characterized the sample by using the following techniques;

- X-rays diffraction (XRD)
- Scanning electron microscope (SEM)
- Infield R-T measurements

3.2.1 X-rays diffraction (XRD)

In crystals, atoms are arranged periodically in regular pattern. These atoms arranged with large number of series in form of parallel planes. By finding distances between atoms and distances between planes, we are able to know about crystal structure, cell parameters of unit cell, crystal structure, structural defects and concentration of impurity of the crystals.

X-rays have very short wavelength, so they have property to penetrate into material and diffract from the atoms of material. The commonly used as target element in X-ray tube for production of x-rays is copper and the wavelength of these rays is about 1.54 Å. When a x-ray having wavelength λ strike on the solid, x-ray diffract from atoms of crystal with angle θ and then detect by detector [2]. The diffraction pattern is explained on the basis of Bragg's Law.

3.2.1.1 Basic principle

When beam of X-ray incident on the crystal and strikes the atoms. It will force the electrons to oscillate as shown in Fig. 3.6. The frequency of the oscillating electrons and incident beam frequency will be identical. In some directions there will be destructive interference which shows the combining rays are out of phase. Contrary to this there will be constructive interference in few directions due to regular and periodic arrangement of atoms. This is due to rays which are in-phase and it has significant impact on the sample. The phenomenon of constructive interference by XRD can be explained by Bragg's Law [3]. The basic working mechanism of XRD is shown in Fig. 3.5.

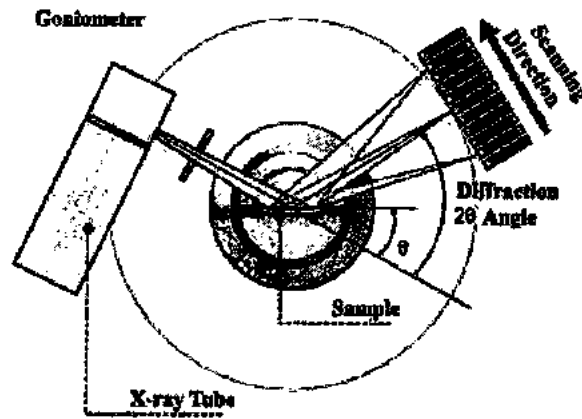


Fig. 3.5: Working mechanism of XRD.

3.2.1.2 Bragg's law

W. L. Bragg and W. H. Bragg was derived the Bragg's Law in 1912. When the wavelength of the x-rays is smaller than the lattice constant, then the x-rays diffract and the direction of diffracted rays different from the direction of incident rays. Diffraction occurs only when Bragg's Law condition satisfied for constructive interference.

Consider parallel planes with interspaced distance d . When x-rays fall on the planes, $2d\sin\theta$ is the path difference for reflected rays. The θ measured form the plane. Constructive interference obtained when the path difference is an integral number m of wavelength λ , so equation is [4];

$$m\lambda = 2d \sin \theta \dots\dots\dots 3.1$$

This is the Bragg's Law. This law satisfied if the wavelength is $\lambda \leq 2d$.

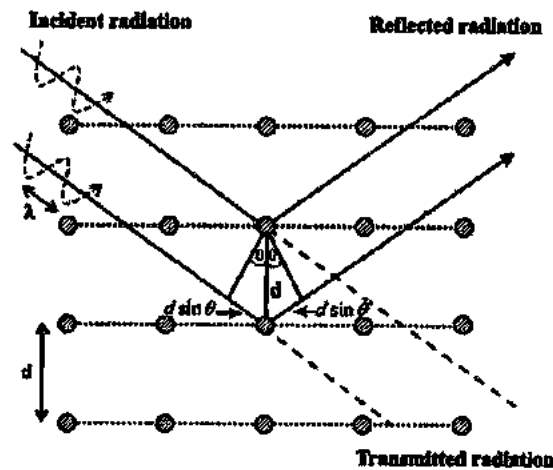


Fig. 3.6: Diffraction of X-rays from crystal planes and illustration of Bragg's Law.

3.2.1.3 Powdered diffraction method

In powdered diffraction method; the powder form of sample is exposed to X-rays. The parameter wavelength ' λ ' or incidents rays remain same while the values of angle ' θ ' change constantly. Mostly superconductors are characterized by using powdered diffraction method. This method also help us to determine the different parameters like interplaner spacing, lattice parameters and diffraction angles.

3.2.1.4 X-rays diffractometer instrument

The main parts of X-rays diffractometer is given below;

➤ **X-Rays Generator:**

This is the source of X-rays. By using different metal, it generates the X-rays.

➤ **Goniometer:**

This part manage the rotation of the counter on which sample is placed.

➤ **Electronic Circuit Panel (ECP):**

ECP electronically detect and count the X-rays [5].

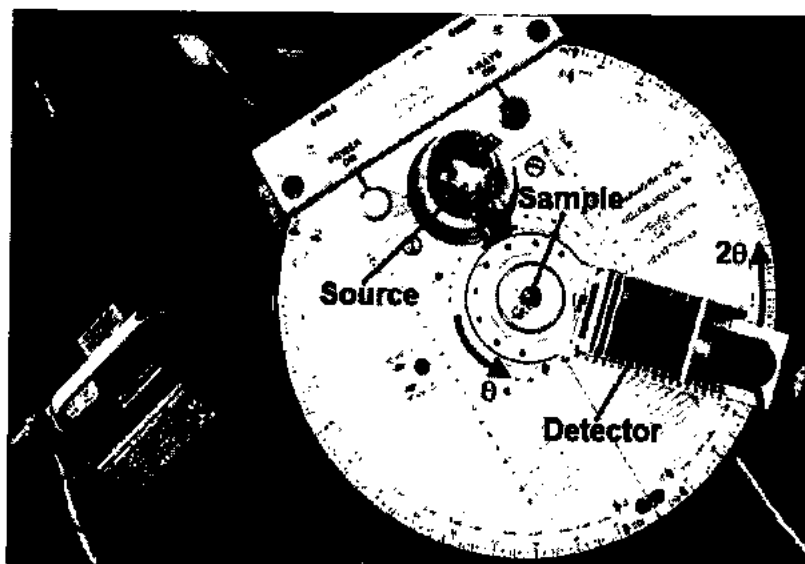


Fig. 3.7: Labeled diagram of X-ray diffractometer.

3.2.1.5 XRD Applications

XRD has many applications in material sciences. The most important applications are

- I. Atomic arrangement can be determined by XRD
- II. Average spacing between two spaces can be measured

- III. Crystalline phases can be determined by XRD
- IV. Integrated intensities can be obtained by XRD
- V. Crystal structure of unknown material can be measured

3.2.2 Scanning electron microscope (SEM)

This is the type of electron microscope. It scans over the surface area of the material and then image formed of that material. Its working is similar to light microscope but the difference is that in light microscope beam of photons is used while in SEM beam of electron is used. SEM has higher resolution as compared to other microscopes. In SEM, an additional technique equipping the x-ray energy dispersive spectrometer (EDS) is use through which we obtain the chemical information of the specimen [6]. The labeled diagram of SEM is shown in Fig.3.8.

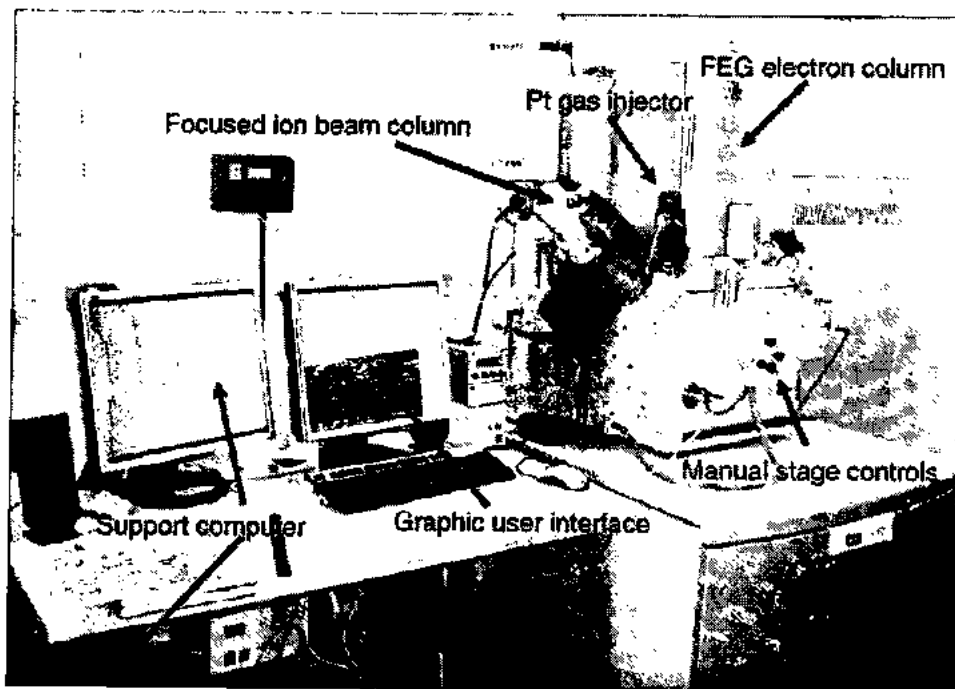


Fig. 3.8: Labeled diagram of scanning electron microscope (SEM).

3.2.2.1 Components of SEM

> Electron Gun

Electron gun is at the very top or the very bottom of the column which provides the intense beam of electrons. These beams of electron achieve from two type of electron gun.

- **Thermionic Gun** Thermal energy provides to the filament (usually used tungsten which has a high melting point) then electrons emitted from the filament and move towards the specimen.
- **Field Emission Gun:** In this electron gun, field is used to eject the electrons from the atoms. This gun is more advanced than thermionic gun.

➤ **Lenses**

These lenses have same function in SEM as in optical microscope. These lenses are used to form clear and detail images. In SEM, lenses are made of magnets and commonly known as condenser lenses. These condenser lenses demagnify the electron beam in order to focus the beam on the target. Another condenser lens is known as objective lens, which is responsible for the size of electron beam that strike on the surface of the sample.

➤ **Scanning System**

Electron beam scanning the sample with a regular manner so, image is formed. The time interval for scanning is so short that we obtained the full image within seconds. To deflect or push the electron beam, scanning coils are used.

➤ **Sample Chamber**

In sample chamber, place the sample which we want to examine. To form the clear image, sample must be in extremely still position, so sample chamber should be insulated from vibrations. SEM is very sensitive that's why usually SEM placed on ground floor of building. Sample chamber also change the angle of the sample.

➤ **Detector**

Detector plays role in SEM as eye in human being. When the electron beam strike on the specimen, the electrons carry information and then detector detect these electrons. Secondary electrons are detected by Everhart-Thorny detector. These detectors produce detailed images. The composition of the sample finds through the x-ray detector and BSE detectors [6, 7].

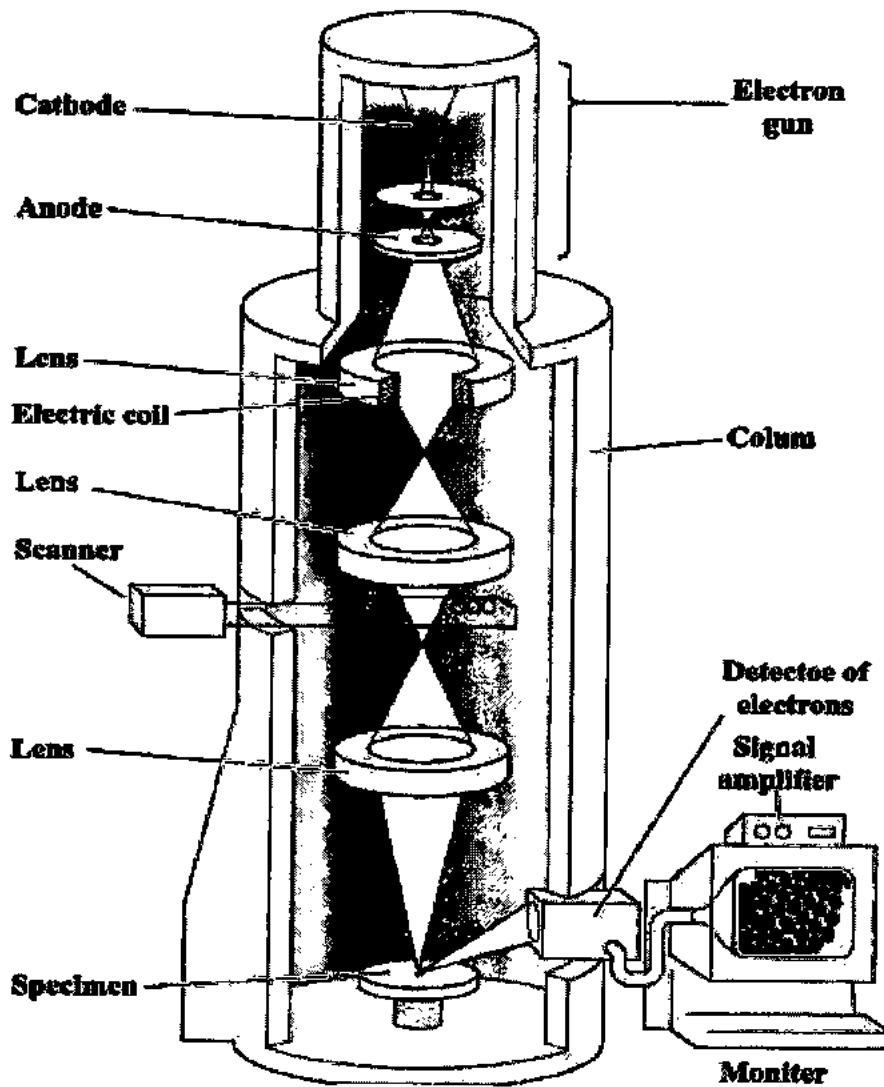


Fig. 3.9: Schematic diagram of scanning electron microscope.

3.2.3 Resistivity measurements by Four-probe method

Conventionally to measure the resistivity of a superconductor, four-probe method is used and through which we can easily find out the critical temperature $T_c(R=0)$. For a conducting material the sources of resistivity are interactions among electrons, atomic vibrations and scattering of electrons caused by defects present in lattices [8].

In Four-probe method all four probes are connected to the surface of rectangular bar shaped sample with help of low resistance contacts. Normally Ohm's law is used for resistivity measurements is;

$$R = \frac{V}{I} \dots\dots\dots 3.2$$

Here V is applied potential and I is current flowing through the sample. The resistance of the sample also depends upon its geometry.

$$R \propto \frac{L}{A} \dots\dots\dots 3.3$$

The resistance R is directly proportional to length L of sample and inversely proportional to area A of sample.

$$R = \rho \frac{L}{A} \dots\dots\dots 3.4$$

Here ρ is the resistivity and it the intrinsic property of a material.

So,

$$\rho = R \frac{A}{L} = \frac{V A}{I I} \dots\dots\dots 3.5$$

The source of constant current is used to apply the current across the outer probes to pass the current through sample and middle probes are used to measured voltage difference between two points. We have applied a current of few milli amperes such as 1 or 2 mA during measuring process. For temperature dependent part of resistivity liquid nitrogen is used which act as cryostat. During measurements of resistivity, temperature is varied from 77 K to room temperature 1 K/min to 3 K/min heat is applied during measurement process [9] and four point probe apparatus is shown in Fig.3.10.

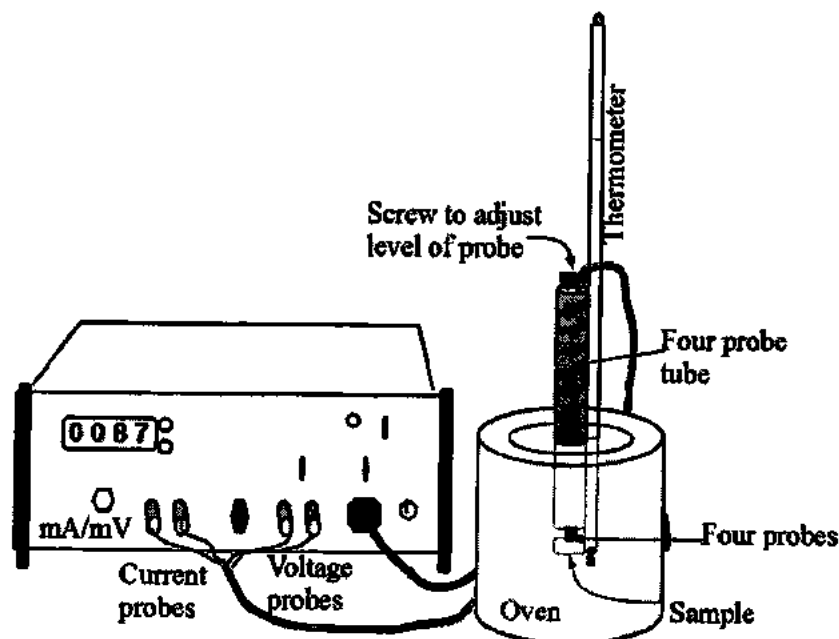


Fig. 3.10: Labeled diagram of four point probe apparatus (R-T measurements).

References

1. Cao, Guozhong, "Synthesis, properties and applications" Imperial college press, London, (2004).
2. G. Gilli, "Fundamentals of Crystallography" Oxford university press, U.K. (2002).
3. B.E. Warren, "X-ray Diffraction" Courier corporation, U.S.A. (1969).
4. C. Kittel "Introduction to solid state physics" 7th ed. Wiley, India (1995)
5. H. P. Klug, and L. E. Alexander, "X-Ray diffraction procedures: for polycrystalline and amorphous materials" 2nd ed. Wiley-interscience, New York (1974).
6. B.Cheney, "Introduction to scanning electron microscopy" San Jose State University press (1995).
7. N.Unakar, J. Tsui, and C. Harding, "Scanning electron microscopy". Ophthalmic research press, U.S.A. (1981).
8. F. Gomory, "Characterization of high-temperature superconductors by AC susceptibility measurements" Supercond. Sci. Technol. **10** (1997) 8.
9. Kleinpenning, "Theory of noise investigations on conductors with the four-probe method" J. Appl. Phys. **48** (1977) 2946

Chapter 4: Results and Discussion

4.1 X-Ray diffraction analysis

Crystal structure and phase purity of $(\text{Ag})_x/\text{CuTi-1223}$ nanoparticles superconductor composites are analyzed by X-ray diffraction (XRD) technique. The XRD spectra of $(\text{Ag})_x/\text{CuTi-1223}$ ($x = 0, 2$ and 4 wt. %) are shown in Fig 4.1. Majority of observed peaks are indexed on the basis of tetragonal structure of CuTi-1223 (space group: $P4/mmm$). The cell parameters (a and c) are determined by Check cell software and incubated that after the addition of Ag nanoparticles, the crystal structure and stoichiometry of $(\text{Ag})_x/\text{CuTi-1223}$ composites are not much affected. The small variations in these cell parameters are due to stresses or strains and little bit distortions have been produced after the addition of Ag nanoparticles in CuTi-1223 matrix.

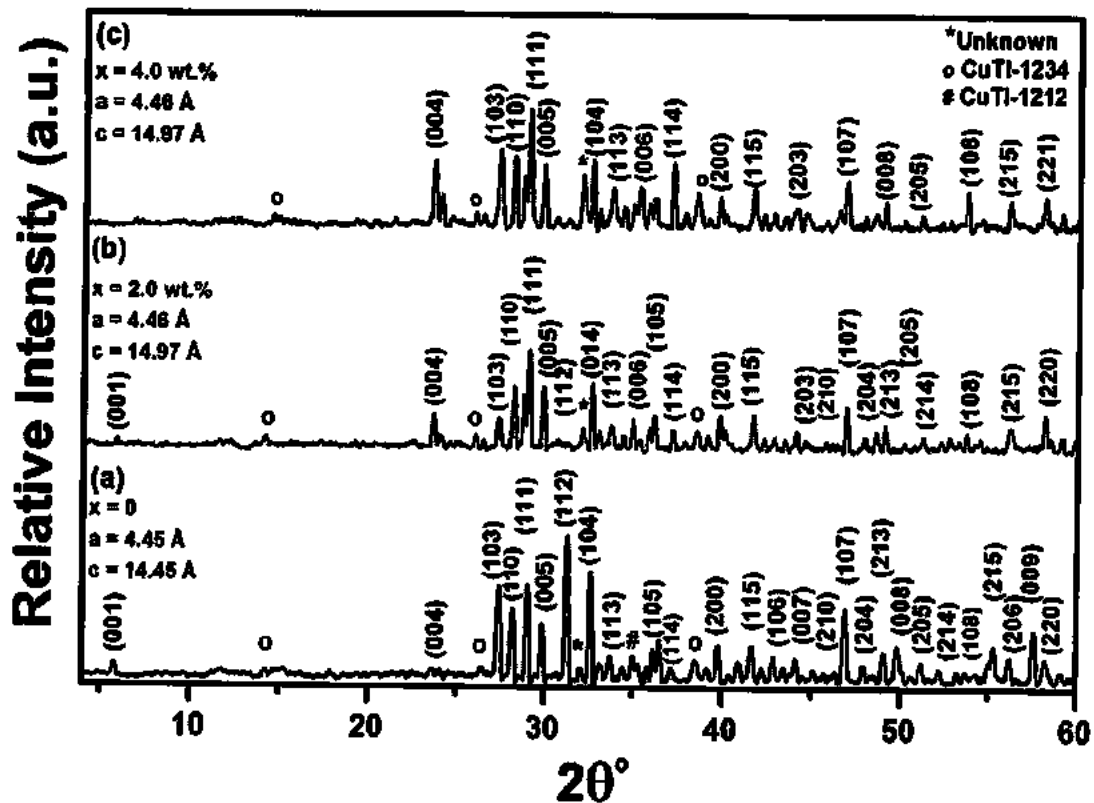


Fig. 4.1: XRD spectra of $(\text{Ag})_x/(\text{CuTi-1223})$ nanoparticles-superconductor composites with $x = 0, 2$ and 4 wt. %.

The slightly shift in diffraction peaks toward greater angle is observed, which may be due to the stresses or strains produced after the addition of Ag nanoparticles. The low intensity un-indexed diffraction peaks in XRD spectra represent the presence of other superconducting phases like CuTi-1234, CuTi-1212 and some unknown impurities.

4.2 Scanning electron microscopy (SEM)

The surface morphology and particle's distribution in superconductor matrix is studied by scanning electron microscopy (SEM) technique. The SEM images of $(Ag)_x/CuTl-1223$ nanoparticles-superconductor composites are shown in Fig. 4.2. The gaps at inter-grain boundaries are well prominent in pure CuTl-1223.

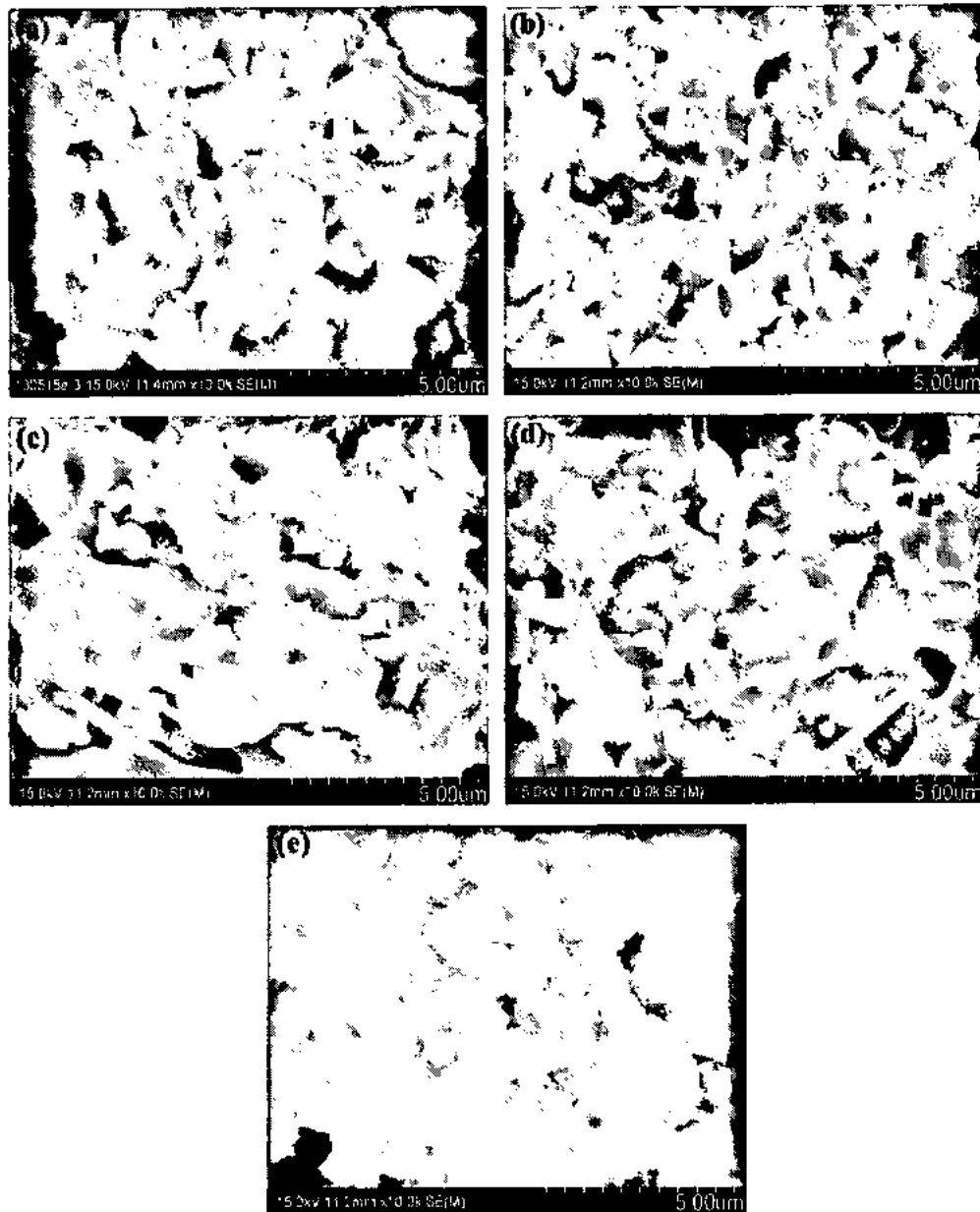


Fig. 4.2: Scanning electron microscopy (SEM) of $(Ag)_x/CuTl-1223$ composites with (a) $x = 0$, (b) $x = 0.5$ wt. %, (c) $x = 1$ wt. %, (d) $x = 2$ wt. % and (e) $x = 4$ wt. %.

The inter-grain connectivity of CuTl-1223 matrix is improved by filling the voids and pores with different concentration of Ag nanoparticles. The small grains of

nanoparticles have been fused together and grow in larger size with the help of activation energy of reaction. The small size grains are also attached to the surface of large size grains and the grains are well connected with each other through Ag nanoparticles.

4.3 Resistive transition

The superconducting transition curves at different applied magnetic field ($H = 0, 2, 4, 6$ and 8 T) for $(Ag)_x/CuTl-1223$ ($x = 0, 0.5, 1.0, 2.0$ and 4.0 wt. %) nanoparticles superconductor composites are shown in Fig. 4.3. The resistive transition widths are sensitive to applied magnetic field and T_c^{onset} is not much affected by magnetic field as reported in high temperature superconductors HTSCs [1, 2]. Whereas normal state resistivity ρ_n is reduced with the inclusion of Ag nanoparticles as compared to pure CuTl-1223 composites. It is clear from the Fig. 4.3 that the zero resistivity critical temperature (T_c) is much affected by applied magnetic field and showing a shift to considerably lower temperature as the applied magnetic field increased. This behavior may attribute to the strong inter-grain pinning energy and seized the vortexes motion near T_c [3]. The value of critical temperature T_c at $H = 0$ T systematically increased with increasing Ag nanoparticles contents and it is found maximum at 101.76 K for $x = 2.0$ wt. %. The resistive transition in CuTl-1223 is strongly influenced by flux dynamics. At low temperature the broadening in transition curve is related to thermally assisted flux flow (TAFF) in magnetic field. The insets of Fig. 4.3 the $\ln(\rho/\rho_0)$ versus $1/T$ of resistivity are named as Arrhenius plots and the activation energies are estimated from the linear portion of these plots at low temperature.

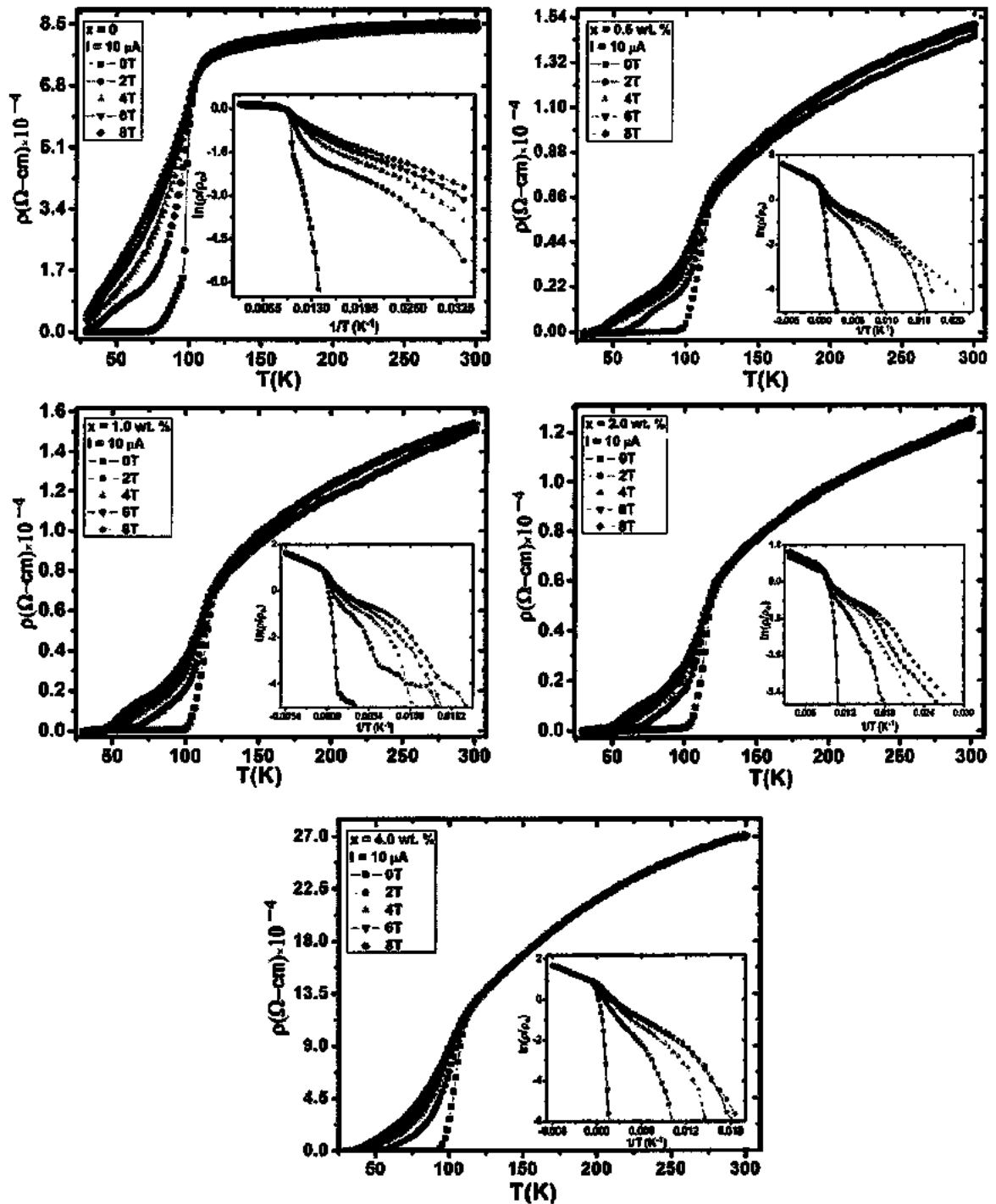


Fig. 4.3: The magnetic field dependence of resistivity as the function of temperature for $(\text{Ag})_x/\text{CuTi-1223}$ nanoparticles-superconductor composites ($x = 0, 0.5, 1.0, 2.0$ and $x = 4.0$ wt. %) at $H = 0, 2, 4, 6$ and 8 T. The inset shows the Arrhenius plots of resistive transition and linear part of low resistivity region is fitted to obtain the activation energy.

4.4 Activation energy

The activation energy U_0 (H, T) plays a vital role as potential energy barrier to keep the magnetic flux in pinning centers and calculated from the Arrhenius plot. Arrhenius law is used to describe the current independent resistivity in thermally assisted flux flow regime [4, 5].

$$\rho = \rho_0 e^{(-U_0/k_B T)} \dots\dots\dots 4.1$$

Where ρ_0 is normal state resistivity, U_0 is activation energy and k_B is Boltzman's constant. The activation energy calculated is shown in Fig. 4.4 and also listed in Table 4.1. It is clearly seen that the activation energy decreases dramatically with the increase in applied magnetic field. The activation energy is also dependent on the Ag nanoparticles contents and it is found optimized for $x = 2$ wt. %. The energy dissipation is due to thermal activation of flux across the pinning barriers.

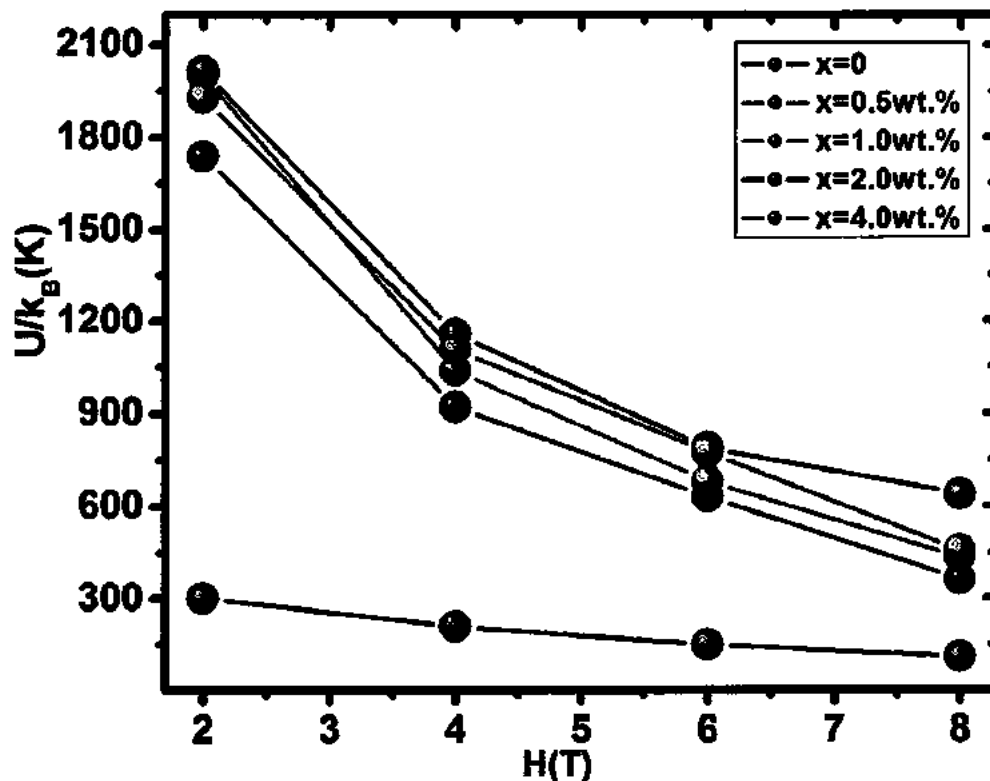


Fig. 4.4: Activation energy versus applied magnetic field plot of $(Ag)_x/CuTi-1223$ nanoparticles-superconductor composites ($x = 0, 0.5, 1.0, 2.0$ and $x = 4.0$ wt. %).

Table 4.1: The magnetic field dependent activation energy $U_o(H)$ is calculated from Arrhenius plots.

| H (T) | 0 | 0.5 wt. % | 1.0 wt. % | 2.0 wt. % | 4.0 wt. % |
|--------------|----------|------------------|------------------|------------------|------------------|
| 2 | 302 | 1739 | 2000 | 2015 | 1928 |
| 4 | 209 | 921 | 1038 | 1158 | 1106 |
| 6 | 149 | 631 | 681 | 788 | 775 |
| 8 | 110 | 361 | 432 | 638 | 456 |

4.5 Upper critical field H_{c2} and irreversibility field H_{irr}

In high temperature superconductors HTSCs the upper critical field H_{c2} is important quantity and it gives the direct information about microscopic parameters like superconducting coherence length ξ , disorders and their anisotropic properties within superconducting state [6, 7]. In HTSCs the upper critical field H_{c2} is mainly determined from resistive transition curves [8, 9]. Some researcher used 90% and 10 % of normal state resistivity ρ_n to estimate the value of upper critical field H_{c2} and irreversibility field H_{irr} [10-12]. The normal state resistivity ρ_n is determined by linearly extrapolating the normal state behavior above onset of superconductivity. The temperature dependence of upper critical field determined from the resistivity measurement at 10%, 50% and 90% of normal state resistivity ρ_n are shown in Fig. 4.5. The upper critical field H_{c2} of composites is increased with increasing the Ag nanoparticles contents and found maximum for $x= 2.0$ wt. %. A higher value of H_{c2} corresponds to stronger flux pinning potential, which indicates the stabilization of flux lines.

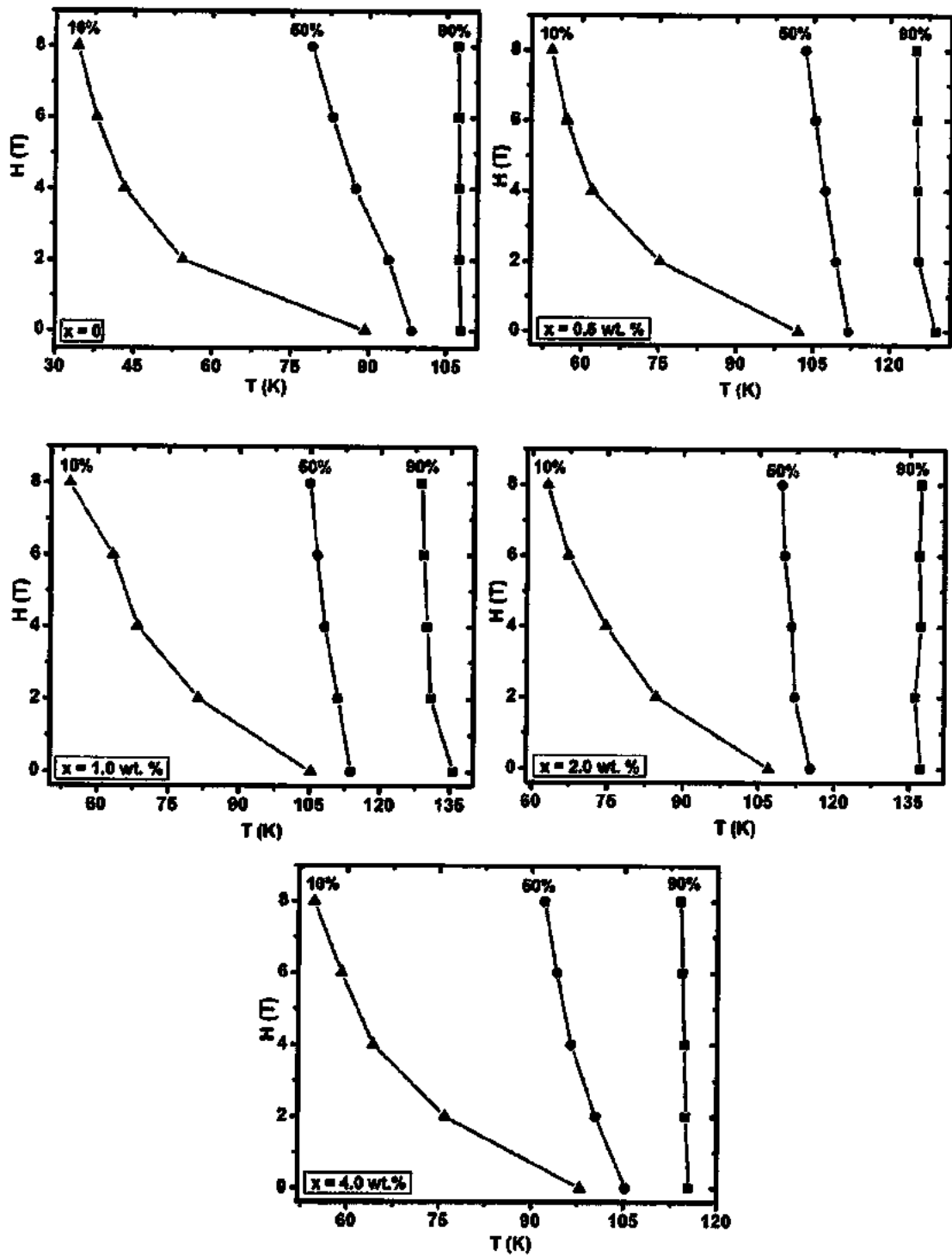


Fig. 4.5: The plot applied field H (T) versus Temperature T (K) for the point where resistivity drop to 90%, 50% and 10% of normal state resistivity ρ_n for $(Ag)_x/CuTl-1223$ nanoparticles-superconductor composites ($x = 0, 0.5, 1.0, 2.0$ and $x = 4.0$ wt. %).

The zero temperature upper critical field $H_{c2}(0)$ is also calculated by using the Werthmer-Helfand-Hohenberg (WHH) formula [13]:

$$H_{c2}(0) = -0.693T_c \left[\frac{dH_{c2}}{dT} \right]_{T=T_c} \dots\dots\dots 4.2$$

$\frac{dH_{c2}}{dT}$ slope values was estimated from magnetic field versus temperature graph and correspond to $x = 0, 0.5, 1.0, 2.0$ and 4.0 wt. % the founded values are $-0.20, -0.191, -0.196, -0.235$ and -0.193 respectively. Using the values of T_c , the values of $H_{c2}(0) = 10.14, 12.66, 13.48, 16.61$ and 12.07 for $x = 0, 0.5, 1.0, 2.0$ and 4.0 wt. % respectively.

In order to approximate the superconducting parameters, Ginzburg-Landau (GL) formula is used to calculate the coherence length $\xi(0)$ at $T = 0K$ [14] :

$$\xi(0) = \sqrt{\frac{\Phi_0}{2\pi H_{c2}(0)}} \dots\dots\dots 4.3$$

Where $\Phi_0 = 2.07 \times 10^{-7}$ Oecm² and $H_{c2}(0)$ is the upper critical field at $T = 0$ K. The graph of $\xi(0)$ and $H_{c2}(0)$ is shown in Fig. 4.6 and the value of T_c , slope of slope $\frac{dH_{c2}}{dT}$, $H_{c2}(0)$ and $\xi(0)$ are given in Table 4.2.

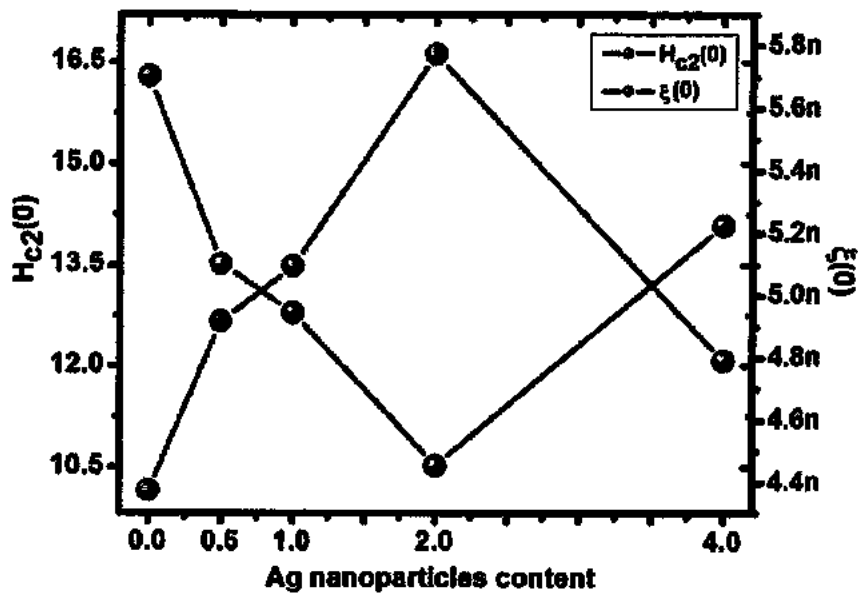


Fig. 4.6: Variations of $H_{c2}(0)$ and $\xi(0)$ with Ag nanoparticles contents.

Table 4.2: Measured superconducting parameters for (Ag)_x/CuTl-1223 nanoparticles-superconductor composites.

| Ag nanoparticles Content | T_c (R=0) (K) | Slope (T/K) | $H_{c2}(0)$ (T) | $\xi(0)$ (Å) |
|--------------------------|-----------------|-------------|-----------------|--------------|
| 0 | 73.23 | -0.20 | 10.14 | 0.570 |
| 0.5 | 95.69 | -0.191 | 12.66 | 0.510 |
| 1.0 | 98.73 | -0.196 | 13.48 | 0.494 |
| 2 | 101.76 | -0.235 | 16.61 | 0.445 |
| 4 | 91.23 | -0.193 | 12.07 | 0.522 |

Conclusions

We studied the vortex dynamics in $Ag_x/CuTl-1223$ nanoparticles-superconductor composites ($x = 0, 0.5, 1.0, 2.0$ and 4.0 wt. %) in presence of magnetic field up to 8 T. The structural investigation revealed that Ag nanoparticles were not incorporated into unit cell of *CuTl-1223* matrix. The magnetic field impact was more pronounced at lower temperature values as a result decreased in the critical temperature (T_c) with increasing the field was observed. The temperature dependent infield dc-resistivity had been explained by thermally activated flux flow (TAAF) model. In conclusion, the superconducting critical temperature T_c , activation energy U_0 and upper critical field H_{c2} were optimized for $x = 2$ wt. %.

References

- [1] D. Sharma, R. Kumar, and V. Awana, "Temperature and field dependence of thermally activated flux flow resistance in $\text{Bi}_2\text{Sr}_2\text{CaCu}_2\text{O}_{8+\delta}$ superconductor" *Solid State Comm.* **152** (2012) 941.
- [2] S. Vinu, P. M. Sarun, R. Shabna, and U. Syamaprasad, "Analysis of thermo-magnetic fluctuations above the glass-transition temperature in $\text{Bi}_{1.6}\text{Pb}_{0.5}\text{Sr}_{2-x}\text{Eu}_x\text{Ca}_{1.1}\text{Cu}_{2.1}\text{O}_{8+\delta}$ ($0.000 \leq x \leq 0.180$) system" *Solid State Sci.* **11** (2009) 1530.
- [3] R. Awad, N. Aly, I. Ibrahim, A. Abou-Aly, and A. Saad, "Effect of magnetic field on the electrical resistance of Tl-1223 doped by Zn and Ni" *Physica B* **307** (2001) 72.
- [4] A. Abou-Aly, M. Mostafa, I. Ibrahim, R. Awad, and M. Al-Hajji, "Electrical and magnetic properties of $\text{Hg}_{0.3}\text{Tl}_{0.7}\text{Ba}_2\text{Ca}_3\text{Cu}_4\text{O}_{10+\delta}$ doped with Ni and Ag" *Supercond. Sci. Technol.* **15** (2002) 938.
- [5] C. Passos, M. Orlando, A. Fernandes, F. Oliveira, D. Simonetti, J. Fardin, H. Belich, and M. Ferreira, "Effects of oxygen content on the pinning energy and critical current in the granular (Hg, Re)-1223 superconductors" *Physica C* **419** (2005) 25.
- [6] S. Celik, K. Ozturk, U. Cevik, and E. Yanmaz, "Investigation of the dependency of the upper critical magnetic field on the content x in $\text{Y}_{1-x}\text{Yb}_{x/2}\text{Gd}_{x/2}\text{Ba}_2\text{Cu}_3\text{O}_{7-y}$ superconducting structures" *J. Alloys Compd.* **460** (2008) 79.
- [7] S. R. Ghorbani, X. Wang, M. Shabazi, S. Dou, K. Choi, and C. Lin, "Flux pinning and vortex transitions in doped BaFe_2As_2 single crystals" *Appl. Phys. Lett.* **100** (2012) 072603.
- [8] M. Oda, Y. Hidaka, M. Suzuki, and T. Murakami, "Anisotropic superconducting properties of $\text{Ba}_2\text{YCu}_3\text{O}_{7-y}$ " *Phys. Rev. B* **38** (1988) 252.
- [9] U. Welp, W. Kwok, G. Crabtree, K. Vandervoort, and J. Liu, "Magnetic measurements of the upper critical field of $\text{YBa}_2\text{Cu}_3\text{O}_{7-\delta}$ single crystals" *Phys. Rev. Lett.* **62** (1989) 1908.
- [10] G. S. Thakur, J. Prakash, M. Kanagaraj, S. Arumugam, and A. K. Ganguli, "Enhancement in superconducting transition temperature (T_c) and upper critical field (H_{c2}) in new Yb-doped $\text{Ce}_{1-x}\text{Yb}_x\text{O}_{0.9}\text{F}_{0.1}\text{FeAs}$ superconductors" *Physica C* **480** (2012) 71.
- [11] A. Yamamoto, J. Jaroszynski, C. Tarantini, L. Balicas, J. Jiang, A. Gurevich, D. Larbalestier, R. Jin, A. Sefat, and M. A. McGuire, "Small anisotropy, weak thermal

fluctuations, and high field superconductivity in Co-doped iron pnictide Ba (Fe_{1-x}Co_x)₂As₂" *Appl. Phys. Lett.* **94** (2009) 062511.

[12] F. Weickert, M. Nicklas, W. Schnelle, J. Wosnitza, A. Leithe-Jasper, and H. Rosner, "Enhancement of the upper critical field in codoped iron-arsenic high-temperature superconductors" *J. Appl. Phys.* **110** (2011) 123906.

[13] N. Werthamer, E. Helfand, and P. Hohenberg, "Temperature and purity dependence of the superconducting critical field, H_{c2}. III. Electron spin and spin-orbit effects" *Phys. Rev.* **147** (1966) 295.

[14] M. Thinkam, "Introduction to Superconductivity" 2nd ed. McGraw-Hill, New York, (1996).